Article

Kinetic Stabilization of an Oligomeric Protein by a Single Ligand Binding Event

R. Luke Wiseman, Steven M. Johnson, Matthew S. Kelker, Ted Foss, Ian A. Wilson, and Jeffery W. Kelly

J. Am. Chem. Soc., **2005**, 127 (15), 5540-5551• DOI: 10.1021/ja042929f • Publication Date (Web): 23 March 2005

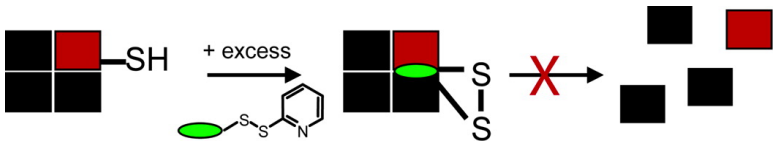

J|A|C|S
ARTICLES
Published on Web 03/23/2005

Kinetic Stabilization of an Oligomeric Protein by a Single Ligand Binding Event

R. Luke Wiseman,[†] Steven M. Johnson,[†] Matthew S. Kelker,[‡] Ted Foss,[†] Ian A. Wilson,[‡] and Jeffery W. Kelly*,[†]

Contribution from the Department of Chemistry, the Department of Molecular Biology, and the Skaggs Institute for Chemical Biology, The Scripps Research Institute, 10550 North Torrey Pines Road, BCC 265, La Jolla, California 92037

Received November 23, 2004; E-mail: jkelly@scripps.edu

Abstract: Protein native state stabilization imposed by small molecule binding is an attractive strategy to prevent the misfolding and misassembly processes associated with amyloid diseases. Transthyretin (TTR) amyloidogenesis requires rate-limiting tetramer dissociation before misassembly of a partially denatured monomer ensues. Selective stabilization of the native TTR tetramer over the dissociative transition state by small molecule binding to both thyroxine binding sites raises the kinetic barrier of tetramer dissociation, preventing amyloidogenesis. Assessing the amyloidogenicity of a TTR tetramer having only one amyloidogenesis inhibitor (I) bound is challenging because the two small molecule binding constants are generally not distinct enough to allow for the exclusive formation of TTR·I in solution to the exclusion of TTR·I_2 and unliganded TTR. Herein, we report a method to tether one fibril formation inhibitor to TTR by disulfide bond formation. Occupancy of only one of the two thyroxine binding sites is sufficient to inhibit tetramer dissociation in 6.0 M urea and amyloidogenesis under acidic conditions by imposing kinetic stabilization on the entire tetramer. The sufficiency of single occupancy for stabilizing the native state of TTR provides the incentive to search for compounds displaying striking negative binding cooperativity (e.g., K_{d1} in nanomolar range and K_{d2} in the micromolar to millimolar range), enabling lower doses of inhibitor to be employed in the clinic, mitigating potential side effects.

Introduction

Extracellular protein misfolding and misassembly is associated with a number of neurodegenerative diseases, including Alzheimer's Disease and the familial amyloidoses.[1−3] Many of these diseases involve the deposition of a polypeptide into fibrous cross β-sheet aggregates, referred to as amyloid.[1,4] Numerous therapeutic strategies have been developed to treat amyloid diseases.[5−7] In cases where proteolytic processing generates the amyloidogenic fragment (e.g., Alzheimer's Disease), small molecule protease inhibitors offer promise.[8,9] In cases where the full-length protein deposits as amyloid, stabilization of the natively folded state by small molecule[10] or protein binding[11,12] is a conservative approach because it avoids formation of the intermediates that have been implicated as being more neurotoxic than the fibrils themselves.[13−17]

Ligand binding to a protein's native state can result in kinetic and/or thermodynamic stabilization, depending on the binding affinity to the native state relative to the misfolding transition state. Selective stabilization of the native state over the denaturation-associated transition state raises the kinetic barrier, slowing the initial misfolding steps associated with amyloid formation. If the kinetic barriers are surmountable, this mode of stabilization also shifts the equilibrium toward the native state under denaturing conditions. Inhibitors that equally stabilize the native state and transition state(s) associated with denaturation shift the equilibrium away from the amyloidogenic conformation(s), decreasing its concentration and therefore the rate of amyloidogenesis owing to the concentration dependence of misassembly.[18]

[†] Department of Chemistry. The Scripps Research Institute.
[‡] Department of Molecular Biology, The Scripps Research Institute.

(1) Buxbaum, J. N. *Curr. Opin. Rheumatol.* **2004**, *16*, 67−75.
(2) Soto, C. *Nat. Rev. Neurosci.* **2003**, *4*, 49−60.
(3) Hardy, J.; Selkoe, D. J. *Science* **2002**, *297*, 353−356.
(4) Petkova, A. T.; Ishii, Y.; Balbach, J. J.; Antzutkin, O. N.; Leapman, R. D.; Delaglio, F.; Tycko, R. *Proc. Natl. Acad. Sci. U.S.A.* **2002**, *99*, 16742−16747.
(5) Cohen, F. E.; Kelly, J. W. *Nature* **2003**, *426*, 905−909.
(6) Ghosh, A. K.; Hong, L.; Tang, J. *Curr. Med. Chem.* **2002**, *9*, 1135−1144.
(7) Dominguez, D. I.; De Strooper, B. *Trends Pharmacol. Sci.* **2002**, *23*, 324−330.
(8) Wolfe, M. S. *Curr. Top. Med. Chem.* **2002**, *2*, 371−383.
(9) Vassar, R. *Adv. Drug Deliv. Rev.* **2002**, *54*, 1589−1602.
(10) Hammarstrom, P.; Wiseman, R. L.; Powers, E. T.; Kelly, J. W. *Science* **2003**, *299*, 713−716.
(11) White, A. R.; Enever, P.; Tayebi, M.; Mushens, R.; Linehan, J.; Brandner, S.; Anstee, D.; Collinge, J.; Hawke, S. *Nature* **2003**, *422*, 80−83.
(12) Peretz, D.; Williamson, R. A.; Kaneko, K.; Vergara, J.; Leclerc, E.; Schmitt-Ulms, G.; Mehlhorn, I. R.; Legname, G.; Wormald, M. R.; Rudd, P. M.; Dwek, R. A.; Burton, D. R.; Prusiner, S. B. *Nature* **2001**, *412*, 739−743.
(13) Reixach, N.; Deechongkit, S.; Jiang, X.; Kelly, J. W.; Buxbaum, J. N. *Proc. Natl. Acad. Sci. U.S.A.* **2004**, *101*, 2817−2822.
(14) Lambert, M. P.; Barlow, A. K.; Chromy, B. A.; Edwards, C.; Freed, R.; Liosatos, M.; Morgan, T. E.; Rozovsky, I.; Trommer, B.; Viola, K. L.; Wals, P.; Zhang, C.; Finch, C. E.; Krafft, G. A.; Klein, W. L. *Proc. Natl. Acad. Sci. U.S.A.* **1998**, *95*, 6448−6453.
(15) Walsh, D. M.; Klyubin, I.; Fadeeva, J. V.; Cullen, W. K.; Anwyl, R.; Wolfe, M. S.; Rowan, M. J.; Selkoe, D. J. *Nature* **2002**, *416*, 535−539.
(16) Volles, M. J.; Lansbury, P. T., Jr. *Biochemistry* **2003**, *42*, 7871−7878.
(17) Sousa, M. M.; Cardoso, I.; Fernandes, R.; Guimaraes, A.; Saraiva, M. J. *Am. J. Pathol.* **2001**, *159*, 1993−2000.

10.1021/ja042929f CCC: $30.25

Transthyretin (TTR) is a homotetrameric protein that transports the small molecule hormone thyroxine (T_4) and *holo*-retinol binding protein in the serum and cerebrospinal fluid (CSF).[19] Over 100 point mutations within the TTR sequence destabilize its structure, predisposing individuals to familial amyloid diseases, including familial amyloid polyneuropathy (FAP), familial amyloid cardiomyopathy (FAC), and CNS selective neurodegeneration.[20−22] Wild-type TTR deposition also results in the late onset disease senile systemic amyloidosis (SSA), leading to cardiac dysfunction in 10% of individuals over age 80.[23]

TTR amyloid fibril formation requires rate-limiting tetramer dissociation and misassembly of partially denatured monomeric subunits.[24−28] Studies on a family in Portugal reveal that kinetic stabilization of the TTR tetramer, comprised in part by disease-associated subunits, is sufficient to prevent pathology.[29] These compound heterozygotes have one allele that codes for the FAP-associated variant V30M TTR and another that codes for a so-called interallelic *trans*-suppressor variant T119M. Inclusion of T119M suppressor subunits into tetramers otherwise composed of V30M subunits raises the kinetic barrier for tetramer dissociation, preventing amyloidosis through transition-state destabilization.[10,30] Because T119M interallelic *trans*-suppression is known to prevent the onset of FAP, we are confident that the selective stabilization of the native state of TTR relative to its dissociative transition state(s) with small molecules will ameliorate pathology by a similar kinetic stabilization mechanism.[10] Since both T_4 binding sites are >98% unoccupied in the serum and CSF,[31] these sites can be utilized for kinetic stabilization.

To date, hundreds of TTR amyloidogenesis inhibitors, spanning a variety of structural classes, have been synthesized.[32−37] Several of these small molecules bind selectively to the two T_4 binding sites in complex biological fluids, imposing kinetic stabilization on TTR. It is established that complete inhibition of TTR amyloidogenesis can be achieved in vitro when both T_4 binding sites are occupied.[10,37] However, it is difficult to discern whether occupancy of only one T_4 site is sufficient to impose kinetic stabilization on the entire tetramer because the inhibitor (I) dissociation constants (K_{d1} and K_{d2}) are too similar to populate the TTR·I state exclusively over the TTR·I_2 and unbound TTR states. To achieve a population of TTR·I above 90%, the K_d's for the T_4 binding sites must be separated by 3 orders of magnitude (Table 1), a requirement not met by the inhibitors characterized to date. Even if this requirement were to be met, it is necessary that the TTR·I population be constant throughout the experiment. The latter requirement is nearly impossible to meet because the denaturing assays used to characterize TTR·I can remove TTR tetramers from solution (by either acid-mediated aggregation or irreversible tetramer dissociation), re-distributing the populations of TTR, TTR·I, and TTR·I_2 in favor of the doubly bound species (TTR·I_2). This re-distribution precludes testing the efficiency of single-site occupancy to prevent TTR aggregation. Despite the difficulties it is worth developing methodology to evaluate TTR·I. Establishing the kinetic stability of TTR·I would provide incentive to search for highly selective inhibitors having a nanomolar K_{d1} and a micromolar or better yet a millimolar K_{d2}.

Table 1. Percentage of Unbound (T), Singly Bound (T·I), and Doubly Bound (T·I_2) TTR Tetramers as a Function of Inhibitor Dissociation Constants[a]

K_{d1}	K_{d2}	% T	% T·I	% T·I_2
100 nM	100 nM	33%	33%	33%
	1 μM	24.20%	60.60%	15.20%
	10 μM	16.20%	79.70%	4.10%
	100 μM	16.80%	82.80%	0.40%
10 nM	10 nM	33%	33%	33%
	100 nM	19.70%	60.60%	19.70%
	1 μM	8.30%	83.30%	8.30%
	10 μM	5.80%	92.80%	1.50%
1 nM	1 nM	33%	33%	33%
	10 nM	19.70%	60.60%	19.70%
	100 nM	8.30%	83.30%	8.30%
	1 μM	3.05%	93.90%	3.05%

[a] Total protein concentration = 3.6 μM; total inhibitor concentration = 3.6 μM.

Covalent tethering of an amyloidogenesis inhibitor to TTR is a convenient approach to evaluate whether occupancy of a single T_4 binding site is sufficient to prevent tetramer dissociation and subsequent amyloidogenesis.[38,39] We demonstrate that occupancy of only one T_4 binding site is sufficient to impose kinetic stabilization on the entire TTR tetramer; therefore, formation of TTR·I should ameliorate human amyloid disease.

Results

Methodology for Tethering a Single Inhibitor to the TTR Tetramer. A high-yield chemo- and regioselective reaction must be employed to covalently label TTR with one amyloidogenesis inhibitor. We have previously taken advantage of the unique reactivity of the Cys-10 sulfhydryl moiety within each subunit, the only Cys within TTR, to modify the TTR tetramer with four small molecules in >90% yield, utilizing a 2-thiopyridine disulfide-activated small molecule.[40] Cys-10 is located at the

(18) Hurshman, A. R.; White, J. T.; Powers, E. T.; Kelly, J. W. *Biochemistry* **2004**, *43*, 7365−7381.
(19) Hamilton, J. A.; Benson, M. D. *Cell Mol. Life Sci.* **2001**, *58*, 1491−1521.
(20) Sekijima, Y.; Wiseman, R. L.; Matteson, J.; Hammarstrom, L.; Miller, S. R.; Sawkar, A. R.; Balch, W. E.; Kelly, J. W. *Cell* **2005**, in press.
(21) Ikeda, S.; Nakazato, M.; Ando, Y.; Sobue, G. *Neurology* **2002**, *58*, 1001−1007.
(22) Saraiva, M. J. *Hum. Mutat.* **2001**, *17*, 493−503.
(23) Westermark, P.; Sletten, K.; Johansson, B.; Cornwell, G. G., III *Proc. Natl. Acad. Sci. U.S.A.* **1990**, *87*, 2843−2845.
(24) Colon, W.; Kelly, J. W. *Biochemistry* **1992**, *31*, 8654−8660.
(25) Kelly, J. W. *Curr. Opin. Struct. Biol.* **1996**, *6*, 11−17.
(26) Kelly, J. W. *Structure* **1997**, *5*, 595−600.
(27) Lai, Z.; Colon, W.; Kelly, J. W. *Biochemistry* **1996**, *35*, 6470−6482.
(28) Liu, K.; Cho, H. S.; Lashuel, H. A.; Kelly, J. W.; Wemmer, D. E. *Nat. Struct. Biol.* **2000**, *7*, 754−757.
(29) Coelho, T.; Carvalho, M.; Saraiva, M. J.; et al. *J. Rheumatol.* **1993**, *20*, 179.
(30) Hammarstrom, P.; Schneider, F.; Kelly, J. W. *Science* **2001**, *293*, 2459−2462.
(31) Bartalena, L.; Robbins, J. *Clin. Lab. Med.* **1993**, *13*, 583−598.
(32) Adamski-Werner, S. L.; Palaninathan, S. K.; Sacchettini, J. C.; Kelly, J. W. *J. Med. Chem.* **2004**, *47*, 355−374.
(33) Klabunde, T.; Petrassi, H. M.; Oza, V. B.; Raman, P.; Kelly, J. W.; Sacchettini, J. C. *Nat. Struct. Biol.* **2000**, *7*, 312−321.
(34) Johnson, S. M.; Petrassi, H. M.; Palaninathan, S. K.; Mohamedmohaideen, N. N.; Purkey, H.; Nichols, C.; Chiang, K. P.; Walkup, T.; Sacchettini, J. C.; Sharpless, K. B.; Kelly, J. W. *J. Med. Chem.* **2005**, *48*, 1576−1587.
(35) Oza, V. B.; Smith, C.; Raman, P.; Koepf, E. K.; Lashuel, H. A.; Petrassi, H. M.; Chiang, K. P.; Powers, E. T.; Sachettinni, J.; Kelly, J. W. *J. Med. Chem.* **2002**, *45*, 321−332.
(36) Razavi, H.; Palaninathan, S. K.; Powers, E. T.; Wiseman, R. L.; Purkey, H. E.; Mohamedmohaideen, N. N.; Deechongkit, S.; Chiang, K. P.; Dendle, M. T.; Sacchettini, J. C.; Kelly, J. W. *Angew. Chem., Int. Ed. Engl.* **2003**, *42*, 2758−2761.
(37) Green, N. S.; Palaninathan, S. K.; Sacchettini, J. C.; Kelly, J. W. *J. Am. Chem. Soc.* **2003**, *125*, 13404−13414.
(38) Hardy, J. A.; Lam, J.; Nguyen, J. T.; O'Brien, T.; Wells, J. A. *Proc. Natl. Acad. Sci. U.S.A.* **2004**, *101*, 12461−12466.
(39) Erlanson, D. A.; Wells, J. A.; Braisted, A. C. *Annu. Rev. Biophys. Biomol. Struct.* **2004**, *33*, 199−223.
(40) Zhang, Q.; Kelly, J. W. *Biochemistry* **2003**, *42*, 8756−8761.

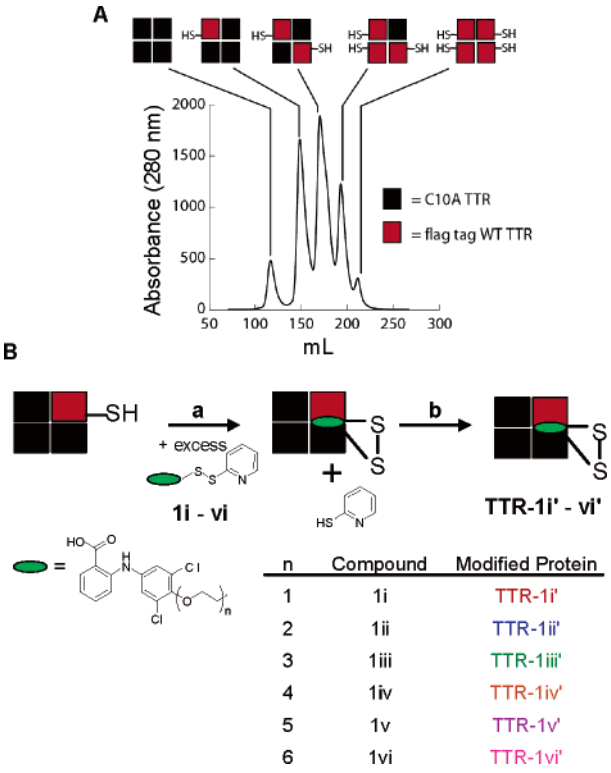

Figure 1. Schematic of the covalent modification procedure. (A) Anion exchange chromatogram of coexpressed C10A/flag-tag WT TTR and the resulting TTR heterotetramers. (B) The (flag-tag WT TTR)$_1$(C10A)$_3$ heterotetramer was incubated with small molecules activated with a 2-thiopyridine moiety (**1i**−**1vi**) at room temperature. (a) Excess small molecule was removed from solution by gel filtration chromatography (b), resulting in TTR tetramers covalently tethered to a single inhibitor. The table defines the nomenclature of the activated inhibitors and the resulting modified heterotetramers prepared from compounds **1i**−**1vi** with varying linker lengths. The prime indicates the inhibitors disulfide tethered to TTR without the 2-thiopyridine-activating moiety.

periphery of the T_4 binding site, making this flexible residue ideal for testing the sufficiency of single occupancy for inhibiting TTR amyloidogenesis. Disulfide tethering of the inhibitor has the added advantage that the linker can be cleaved with DTT, allowing control experiments requiring free ligand.

To achieve monolabeling, a tetrameric species must be prepared that contains only one Cys-bearing TTR subunit. TTR heterotetramers of defined stoichiometry have been prepared previously, utilizing one subunit that has a distinguishing 16-residue N-terminal tandem flag-tag (DYKDDDDKDYKD-DDDK).[10,41] Coexpressing flag-tag WT TTR and TTR containing the point mutation C10A results in a statistical distribution of heterotetramers from which the (flag-tag WT)$_1$(C10A)$_3$ tetramer can be separated from the other four resolvable tetramers using anion-exchange chromatography (Figure 1A). The 2,2,2 symmetry of the TTR tetramer renders all (flag-tag WT)$_1$(C10A)$_3$ heterotetramers equivalent. Importantly, the (flag-tag WT)$_1$(C10A)$_3$ heterotetramer appears to be kinetically stable at 37 °C for at least 24 h, preventing reequilibration (Figure 1A). Incubation of (flag-tag WT)$_1$(C10A)$_3$ with a 2-thiopyridine disulfide-activated amyloidogenesis inhibitor (e.g., **1i**−**vi**) will result in the formation of TTR tetramers covalently labeled at one subunit (Figure 1B).[40]

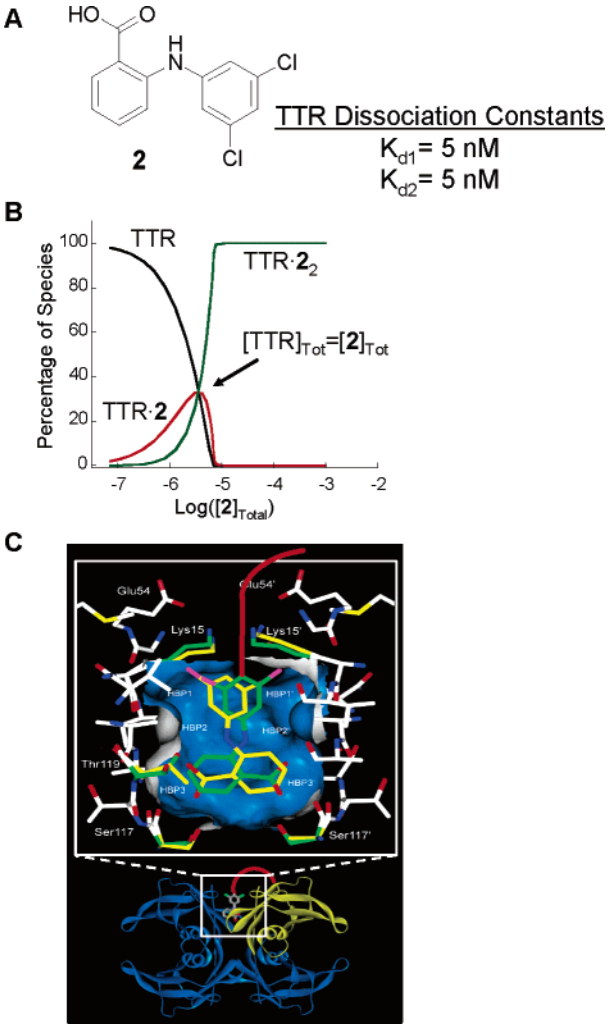

Figure 2. Structure of compound **2** bound to TTR reveals an accessible position for covalent attachment to TTR. (A) Chemical structure of compound **2**. (B) The percentage of unbound (TTR; black), singly bound (TTR·**2**; red), and doubly bound (TTR·**2**$_2$; green) TTR as a function of the concentration of **2**. The arrow indicates the position of the curve where the concentration of the TTR tetramer is equal to the concentration of **2**. (C) Crystal structure of TTR·**2**$_2$ demonstrating the suitability and accessibility of the *para*-position to mediate tethering to TTR (red line). Adapted from ref 35.

The small molecule selected for tethering in this experiment (2-(3,5-dichlorophenylamino)benzoic acid (**2**)) is one of the most efficacious TTR amyloidogenesis inhibitors characterized to date (Figure 2A; $K_{d1} = K_{d2} = 5$ nM).[10,35] Unfortunately, these dissociation constants prevent the population of TTR·I to the exclusion of TTR and TTR·I$_2$ at equimolar concentrations of free ligand and TTR tetramer (Figure 2B). The crystal structure of TTR·**2**$_2$ demonstrates that the *para*-position of the dichlorinated phenyl ring points directly out of the binding pocket into the solvent (Figure 2C),[35] presenting an ideal site for tether attachment. Incorporation of a *para*-phenol enables poly(ethylene glycol) (PEG) chains of variable length to be attached onto **2** (Scheme 1). These *para*-pegylated analogues of **2** (**5a**−**f**) inhibit TTR aggregation as effectively as **2** in an acid-mediated amyloidogenesis assay (Figure 3), suggesting that PEG linkers will be effective for tethering this inhibitor to the TTR tetramer via a disulfide-forming reaction as outlined above. Computer modeling taking into account the flexibility of the Cys-10 residue suggests that a PEG linker of 14−21 Å

(41) Schneider, F.; Hammarstrom, P.; Kelly, J. W. *Protein Sci.* **2001**, *10*, 1606−1613.

Scheme 1. Synthesis of Compounds To Evaluate the Feasibility of Covalent Tethering at the *para*-Position[a]

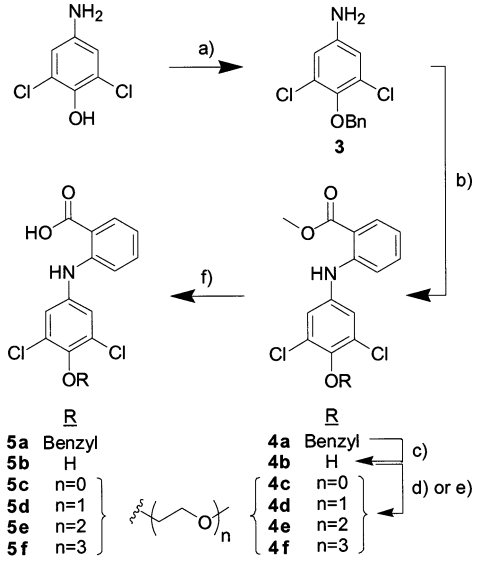

[a] Reagents and conditions: (a) Benzyl bromide, K_2CO_3, acetone (66%); (b) methyl 2-bromobenzoate, $Pd_2(dba)_3$, BINAP, Cs_2CO_3, toluene, reflux (68%); (c) 10% Pd/C, H_2, 1:1 MeOH:EtOAc (97%); (d) MeI, K_2CO_3, DMF (73%); (e) $HO(CH_2CH_2O)_nMe$ ($n = 1-3$), PPh_3, DIAD, THF (72−89%); (f) $LiOH{\cdot}H_2O$, 3:1:1 THF:MeOH:H_2O (74−100%).

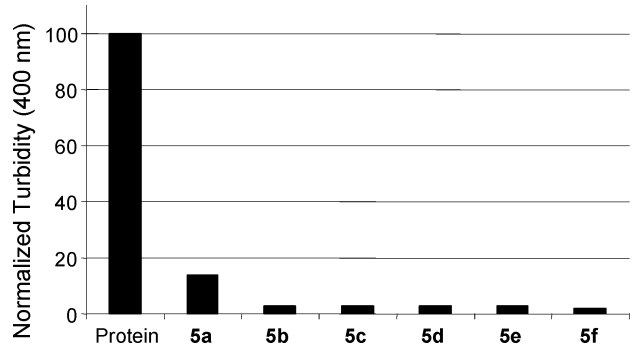

Figure 3. Acid-mediated (pH 4.4) fibril formation of WT TTR (3.6 μM) in the presence of untethered inhibitors **5a**−**f** (7.2 μM, 72 h). The turbidity was measured at 400 nm, normalizing the signal to WT TTR in the absence of small molecule.

comprising 4−6 PEG units would be optimal; therefore, a range of linkers was evaluated (Figure 1B).

Although reaction of 2,2′-dithiodipyridine with 2-mercaptoethanol was found to efficiently produce the shortest activated disulfide linker (**9i**, $n = 1$, 67%),[40] the lack of longer commercially available monomercaptopoly(ethylene glycol)s necessitated synthetic methodology to make these linkers (Scheme 2). Commercially available poly(ethylene glycol)s ($n = 1-6$) were protected as monobenzoates, brominated,[42] and subjected to nucleophilic attack by thioacetic acid affording acetylsulfanylpoly(ethylene glycol) benzoates in good overall yields (**8i**−**vi**, 51−67%, Scheme 2). Methanolysis of the ester and thioester protecting groups followed by thiol activation with 2,2′-dithiodipyridine afforded the linkers (**9i**−**vi**) in moderate yields (23−45%).[40,43] The activated linkers were then coupled (76−98%) to compound **12** via Mitsunobu reactions, taking care to

(42) Hammerschmidt, F.; Kahlig, H. *J. Org. Chem.* **1991**, *56*, 2364−2370.
(43) DeVries, V. G.; Moran, D. B.; Allen, G. R.; Riggi, S. J. *J. Med. Chem.* **1976**, *19*, 946−957.

Scheme 2. Synthesis of 2-Mercaptopyridine-Activated Disulfide Linkers[a]

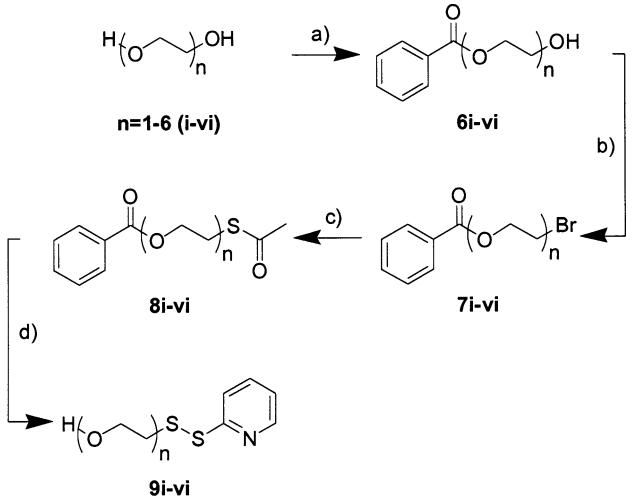

[a] Reagents and conditions: (a) Benzoyl chloride, pyridine, CH_2Cl_2 (65−82%); (b) NBS, PPh_3, CH_2Cl_2 (79−99%); (c) thioacetic acid, NaH, DMF (75−94%); (d) 2,2′-dithiodipyridine, sodium methoxide (0.5 M in methanol), methanol (23−45%).

Scheme 3. Synthesis of the Inhibitors Activated for Disulfide Tethering[a]

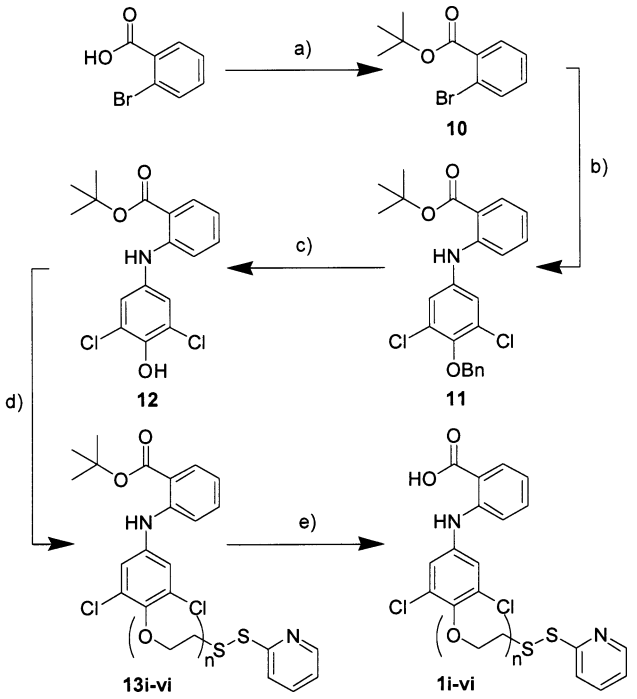

[a] Reagents and conditions: (a) *tert*-BuOH, DCC, DMAP, CH_2Cl_2 (61%); (b) 4-benzyloxy-3,5-dichloroaniline (**3**), $Pd_2(dba)_3$, BINAP, Cs_2CO_3, toluene, reflux (58%); (c) 10% Pd/C, H_2, 1:1 MeOH:EtOAc (89%); (d) **9i**−**vi**, PPh_3, DIAD, THF (85−91%); (e) TFA (100%).

preactivate the triphenylphosphine with diisopropyl azodicarboxylate prior to linker addition to avoid reduction of the activated disulfide bond (Scheme 3). The methyl ester utilized in Scheme 1 was changed to a *tert*-butyl ester because the 2-thiopyridine-activated disulfide group proved labile under the alkaline conditions required to saponify the methyl ester. The activated disulfide survives under the acidic conditions required to liberate the *tert*-butyl ester protecting group (Scheme 3, step e), affording the desired covalent inhibitor precursors (**1i**−**vi**) in quantitative yields.[44]

Covalent Tethering of Small Molecules to TTR Is Mediated by Disulfide Bond Formation. TTR-1i′−TTR-1vi′ were prepared by incubating the (flag-tag WT)$_1$(C10A)$_3$ heterotetramer with an excess of activated inhibitors (**1i**−**vi**) (Figure 1B, step a, 2 h, 25 °C). The excess small molecule was removed by gel filtration chromatography, yielding inhibitors disulfide tethered to the TTR heterotetramer (**TTR-1i′**−**TTR-1vi′**) in >80% yield (Figure 1B, step b). Removal of **1i**−**vi** from solutions of **TTR-1i′**−**TTR-1iv′** could be verified by HPLC in every case except for **TTR-1iv′**, where the modified flag-tag WT subunit of **TTR-1iv′** coeluted with the reduced untethered molecule **1iv^{SH}**. It is unlikely that a significant amount of free **1iv** is present after gel filtration, as demonstrated in Figure 4 (see below). Mixed disulfide formation was monitored by HPLC under conditions that denature the heterotetramer into individual subunits, revealing labeling of the flag-tag WT TTR subunit with the inhibitor (cf. Figure 4A and B). Integration of the HPLC peaks corresponding to C10A subunits and the modified flag-tag WT TTR subunit of **TTR-1iv′**, correcting for the difference in molar absorptivity between the C10A and the modified flag-tag WT TTR subunit of **TTR-1iv′**, demonstrates a distribution of ∼3:1 (Figure 4B) as expected. LC-MS demonstrated that only the flag-tag WT TTR subunits were modified and not the C10A subunits (data not shown). Upon treatment of the covalently labeled sample with 1 mM DTT, the covalently modified protein completely reverted to its unlabeled state (Figure 4C). Integration of the HPLC peaks corresponding to C10A TTR subunits and flag-tag WT TTR subunits after DTT treatment remains 3:1, verifying the reversibility of the tether attachment (cf. Figure 4A and C). The demonstrated ability of gel filtration to remove aromatic inhibitors by adsorption, the 3:1 ratio of C10A and modified flag-tag WT TTR subunits of **TTR-1iv′** after reduction, and the substantially different amyloidogenicity and tetramer dissociation exhibited by untreated and DTT-treated samples make it unlikely that any untethered inhibitor is present in solutions of **TTR-1iv′**. During inhibitor tethering ∼10% of flag-tag WT TTR was converted to a byproduct, indicated by the small right-most peak of the HPLC trace (Figure 4B). LC-MS could not detect this product, which is likely the 2-thiopyridine disulfide adduct, consistent with the disappearance of this peak upon DTT reduction (Figure 4C).

Inhibitor Tethering Does not Disturb TTR's Native Structure. Tethering small molecules to TTR could alter its tertiary and/or quaternary structure. Hence, the far-UV circular dichroism (CD) spectra of TTR·I conjugates were compared to (flag-tag WT)$_1$(C10A)$_3$ TTR, demonstrating that the β-sheet content remains unchanged (Figure 4D). The slight difference in intensity is most likely a result of a change in the molar absorptivity associated with inhibitor tethering. TTR·I conjugates with linkers that are too short or too long to allow for efficient intramolecular binding could result in oligomerization by tethered inhibitor binding to a T_4 site in another tetramer. Therefore, all of the TTR·I conjugates (**TTR-1i′**−**TTR-1vi′**) were subjected to sedimentation velocity analytical ultracentrifuge experiments (Supporting Information, Figure 1). In all cases the conjugates were tetrameric. No intermolecular binding was observed based on the absence of structures larger than tetramers.

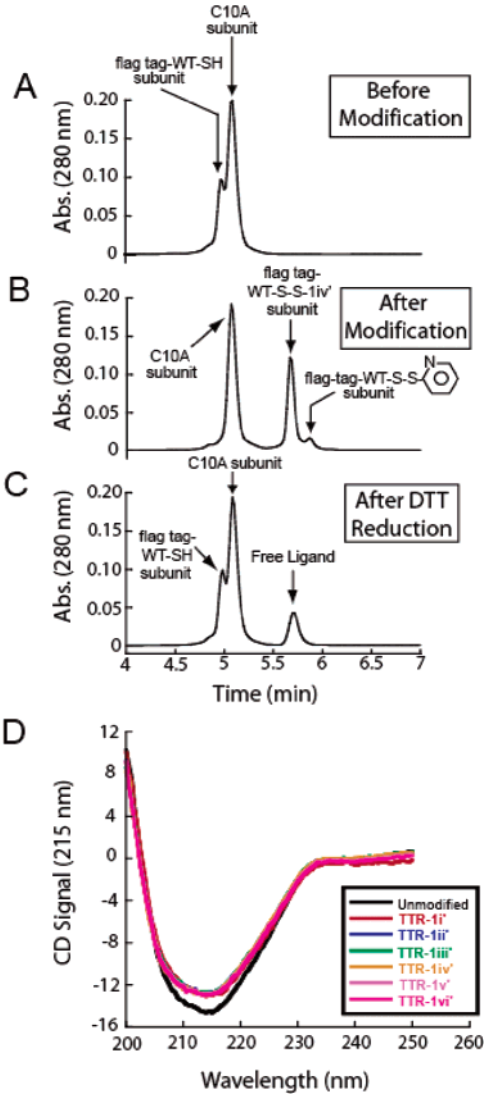

Figure 4. HPLC traces of the unmodified heterotetramer ((flag-tag WT)$_1$-(C10A)$_3$), a covalently modified TTR heterotetramer (**TTR-1iv′**), and a covalently modified TTR heterotetramer (**TTR-1iv′**) treated with DTT under denaturing conditions. (A) Representative HPLC trace of the monomeric subunits from the unmodified heterotetramer (flag-tag WT TTR)$_1$(C10A)$_3$. Integration of C10A subunits relative to flag-tag WT TTR subunits (corrected for the difference in molar absorptivity between flag-tag WT and C10A subunits) is 2.8:1. (B) Representative HPLC trace of monomeric subunits from the modified heterotetramer **TTR-1iv′**. Integration of C10A subunits relative to the modified flag-tag WT subunits from **TTR-1iv′** (corrected for the difference in molar absorptivity between the modified flag-tag WT subunit from **TTR-1iv′** and C10A subunits) reveals a ratio of 3:1. (C) Representative HPLC trace of monomeric subunits from the modified heterotetramer **TTR-1iv′** incubated with 1 mM DTT demonstrating the reversibility of the disulfide attachment. The peaks corresponding to free small molecule (**1iv^{SH}**) and the modified flag-tag WT TTR subunit of **TTR-1iv′** are found to elute at the same retention time, making it difficult to discern the disappearance of the modified flag-tag WT TTR subunit from **TTR-1iv′** upon treatment with DTT. However, a 3:1 ratio of the integrations for the C10A subunits relative to the unmodified flag-tag WT TTR subunits is observed upon DTT reduction, demonstrating that the reduction is quantitative. The elution time of other reduced small molecules (**1i^{SH}**−**1vi^{SH}**) is distinct from the modified flag-tag WT TTR subunits of **TTR-1i′**−**TTR-1iv′**, allowing this analysis to be made. (D) CD spectra of modified and unmodified TTR heterotetramers demonstrating that the small-molecule attachment has little effect on the secondary structure of the tetrameric protein ((flag-tag WT TTR)$_1$(C10A)$_3$, black; **TTR-1i′**, red; **TTR-1ii′**, blue; **TTR-1iii′**, green; **TTR-1iv′**, orange; **TTR-1v′**, purple; **TTR-1vi′**, pink).

(44) Hayword, M. M.; Adrian, J. C.; Schepartz, A. *J. Org. Chem.* **1995**, *60*, 3924−3927.

Table 2. Data Processing and Refinement Statistics for the **TTR-1iv′** Crystal Structure (Figure 5)

resolution range (outer shell)	30−1.69 Å (1.76−1.69 Å)
unique reflections	26 531 (2795)
completeness	96.5% (88.5%)
redundancy	3.4 (2.3)
R_{sym}[a]	6.0% (60.7%)
average $I/\sigma(I)$	33.2 (2.3)
refinement	
resolution range (outer shell)	27.63−1.69 Å (1.73−1.69 Å)
R_{cryst}[b]	21.7% (33.7%)
R_{free}[b]	23.9% (36.3%)
protein atoms/water molecules/ligand molecules	1712/104/42
coordinate error[c]	0.084 Å
rmsd bonds (angles)	0.015 Å (1.55°)
$\langle B \rangle$ protein atoms/water molecules/ligand molecules	16.2 Å^2/32.6 Å^2/41.9 Å^2
Ramachandran statistics	
additional allowed	7.4%
most favored	92.6%

[a] $R_{sym} = 100 \cdot \sum_h \sum_i |I_i(h) - \langle I(h) \rangle| / \sum_h I(h)$, where $I_i(h)$ is the ith measurement of the h reflection and $\langle I(h) \rangle$ is the average value of the reflection intensity. [b] $R_{cryst} = \sum |F_o| - |F_c| / \sum |F_o|$, where F_o and F_c are the structure factor amplitudes from the data and the model, respectively. R_{free} is R_{cryst} with 5 % of test set structure factors. [c] Based on Maximum Likelihood.

Crystal Structure of the TTR-1iv′ Conjugate Verifies Intramolecular Binding to the T_4 Site. The crystal structure of the **TTR-1iv′** conjugate reveals a unimolecular binding mode that is virtually identical to that of the untethered TTR·**2**$_2$ complex (cf. Figures 2C and 5A). The 1.69 Å model (R_{cryst} = 21.7%, R_{free} = 23.9%, Table 2) reveals that 92.6% of the residues are in the most favored region of the Ramachadron plot while the remainder are in an allowed region. The first nine residues, the last three residues, the 16 residues of the flag-tag, as well as the PEG linker tethering the inhibitor to Cys-10 were all too flexible to provide interpretable electron density. Because **TTR-1iv′** crystallized in the $P2_12_12_1$ space group, there is a random distribution of occupied and unoccupied sites in the crystal; therefore, each T_4 binding site exhibits partial occupancy. There are two symmetry-related binding modes observed in all TTR cocrystal structures due to a C_2 axis of symmetry running through the center of the T_4 sites—these modes were observed in the structure of **TTR-1iv′**. The superimposition of the **TTR-1iv′** structure with the *apo*-TTR crystal structure (Figure 5B) reveals a high level of structural homology, with rmsd's for main chain and all atoms of 0.19 and 0.74 Å, respectively. The conformations adopted by residues comprising the T_4 binding site are identical to those of *apo*-WT TTR. Dissolution of the **TTR-1iv′** crystal followed by HPLC analysis reveals that crystallization did not sever the tether.

Occupancy of One T_4 Binding Site Effectively Prevents TTR Aggregation Including Amyloidogenesis. TTR can be induced to form aggregates and amyloid via partial acid denaturation.[24,27] Aggregation, as measured by turbidity, is maximal over the pH range of 4.0−4.8. The best inhibitors block >90% of aggregation at a concentration twice that of the protein concentration (7.2 μM). Tethering one inhibitor to the T_4 site allows us to test the amyloidogenicity of TTR·I conjugates and evaluate the sufficiency of one binding event to impose kinetic stabilization on the entire tetramer.

The efficacy of the tethered inhibitors is highly dependent on the length of the linker, which likely correlates with the extent of T_4 site occupancy. Incorporation of a single PEG unit into the linker (**TTR-1i′**) affords a conjugate that was almost as amyloidogenic as WT TTR at pH 4.4 (Figure 6A), consistent with modeling indicating that this linker would be too short to allow sustained binding of the small molecule to the T_4 site. Doubling the length of the PEG linker to two units (**TTR-1ii′**) slightly decreases aggregation; however, the pH optimum of **TTR-1ii′** aggregation is similar to that of (flag-tag WT)$_1$(C10A)$_3$ TTR, suggesting that the occupancy of small molecule in the T_4 binding site was low. Increasing the linker length to 3−6 PEG units (**TTR-1iii′**−**TTR-1vi′**) markedly decreased amyloidogenicity as compared to (flag-tag WT)$_1$(C10A)$_3$ TTR. The small amount of aggregation observed (<15%) from **TTR-1iii′**−**TTR-1vi′** is consistent with the fraction of TTR tetramer lacking a tethered inhibitor (see below), implying that occupancy of one T_4 binding site prevents amyloidogenesis.

Reducing the disulfide within the tether using DTT allows the activity of the untethered inhibitors to be assessed. Incubating **TTR-1i′**−**TTR-1vi′** at pH 4.4 with 1 mM DTT resulted in ~30% fibril formation (Figure 6B; red symbols), very similar to the extent of aggregation allowed by **2** (Figure 6B, dashed red line),[10] indicating that the PEG linker is rather innocuous. The reduced inhibitors are more effective than their tethered counterparts in the case of **TTR-1i′** and **TTR-1ii′**, likely owing to the strain induced by the short linker. In contrast, the tethered inhibitors containing 3−6 PEG units are much more effective than their untethered counterparts (Figure 6B, compare red and black symbols).

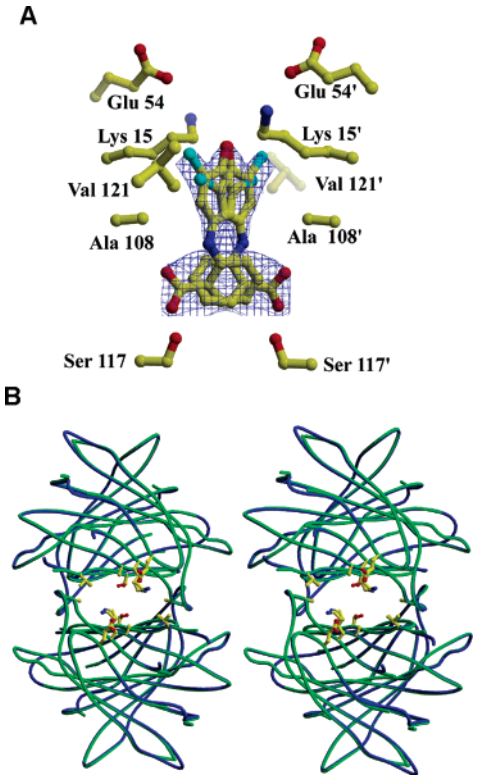

Figure 5. (A) Crystal structure of **TTR-1iv′** demonstrating that the covalently attached small molecule can bind to the T_4 binding site. One of the two hormone binding sites at the dimer interface of **TTR-1iv′** is shown depicting the two symmetry-related binding modes. Ligand density is from a $3F_o - 2F_c$ simulated annealing-omit map in both binding modes and is contoured at 1.0 σ. (B) Stereoview of an overlay of *apo*-TTR (green) and **TTR-1iv′** (blue). The residues represented by the stick model are identical to those in Figure 5A.

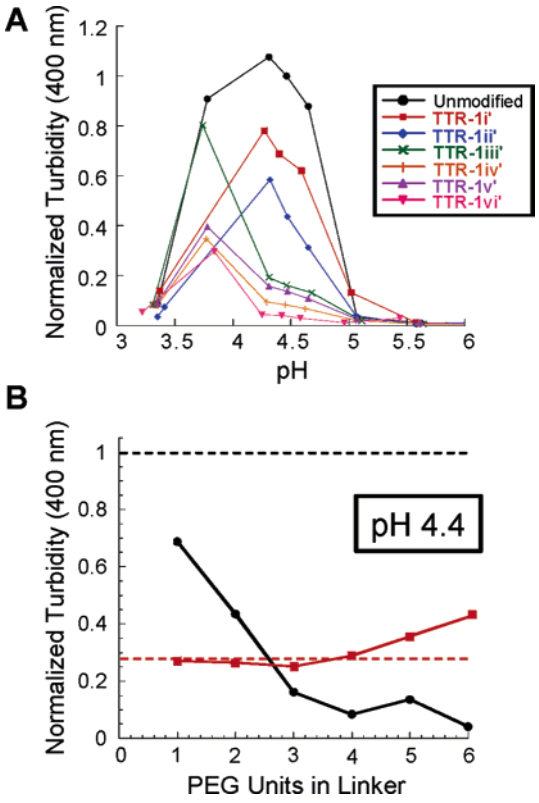

Figure 6. Assessing the amyloidogenicity of **TTR-1i′**−**TTR-1vi′**. (A) Acid-mediated aggregation of **TTR-1i′**−**TTR-1vi′** (3.6 μM) as a function of pH and the length of the PEG linker. The extent of fibril formation was normalized to the unmodified heterotetramer at pH 4.4 ((flag-tag WT TTR)$_1$-(C10A)$_3$, -black circles; **TTR-1i′**, red squares; **TTR-1ii′**, blue diamonds; **TTR-1iii′**, green ×; **TTR-1iv′**, orange crosses; **TTR-1v′**, purple triangles; **TTR-1vi′**, pink upside down triangles). (B) Fibril formation (pH 4.4) of **TTR-1i′**−**TTR-1vi′** in the absence (black) and presence (red) of 1 mM DTT. Proteins with a tethered inhibitor clearly show a dependence on the linker length, which is lost upon reduction with DTT. The dotted lines represent the amyloidogenicity of the control heterotetramer ((flag-tag WT TTR)$_1$(C10A)$_3$; 3.6 μM) in the absence of small molecule (black) and in the presence of compound **2** (3.6 μM) lacking a tether (red).

A Single Tethered Inhibitor Dramatically Slows Tetramer Dissociation. The rate of TTR tetramer dissociation is followed by linking the slow tetramer dissociation process to the much faster monomer unfolding event, monitored by circular dichroism (CD) spectroscopy under denaturing conditions.[45] This approach has been used previously to determine the extent of kinetic stabilization of the TTR tetramer as a function of inhibitor concentration.[10,32,36] The best untethered small molecules completely inhibit dissociation in 6.0 M urea when incubated at a concentration (3.6 μM) twice that of the TTR tetramer (1.8 μM).[10] Reducing the concentration of these small molecules does not allow us to conclude anything about the extent to which single inhibitor occupancy imposes kinetic stabilization on TTR for the reasons discussed in the Introduction.

The TTR tetramer dissociation rates from **TTR-1i′** and **TTR-1ii′** were only slightly slower (0.032 and 0.019 h^{-1}, respectively) than the unmodified heterotetramer control (0.042 h^{-1}), suggesting that the short linkers lead to inefficient inhibitor binding (Figure 7A and B). Lengthening the covalent linker to 3−6 PEG units (**TTR-1iii′**−**TTR-1vi′**) afforded tetramers displaying very

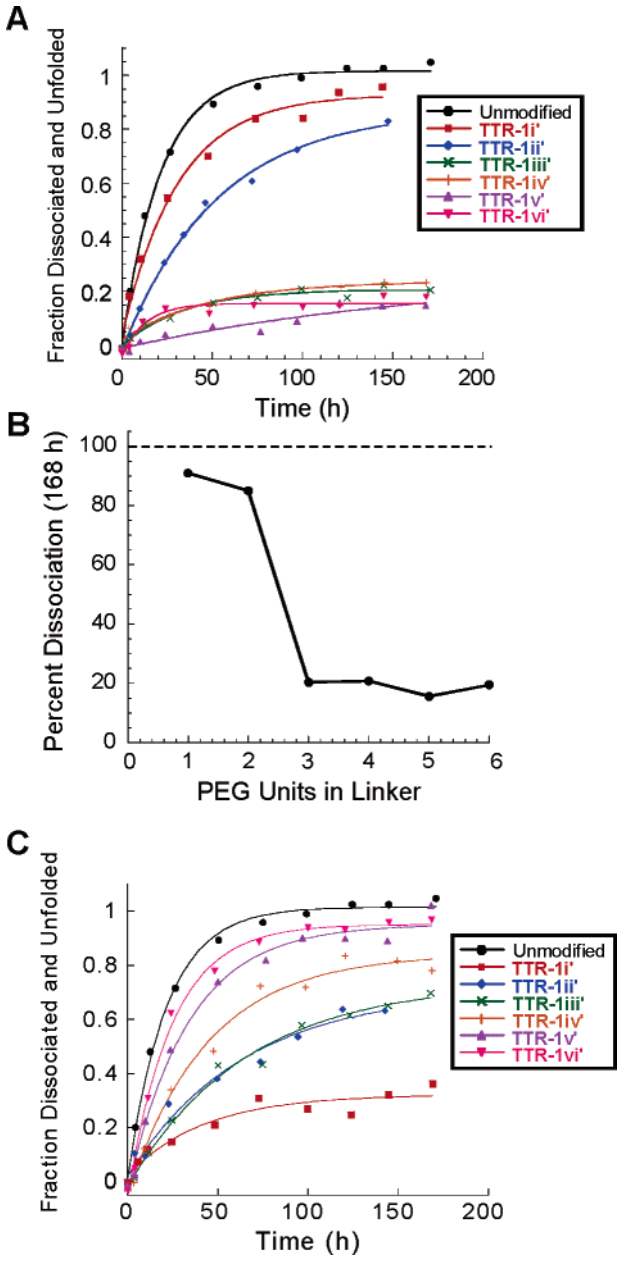

Figure 7. Assessing TTR tetramer dissociation kinetics in 6.0 M urea. (A) The dissociation kinetics of **TTR-1i′**−**TTR-1vi′** in 6.0 M urea was revealed by monitoring the CD signal at 215 nm. Only the longer linkers allow sustained binding of the ligand to the T_4 binding site and inhibition of tetramer dissociation ((flag-tag WT TTR)$_1$(C10A)$_3$, black circles; **TTR-1i′**, red squares; **TTR-1ii′**, blue diamonds; **TTR-1iii′**, green ×; **TTR-1iv′**, orange crosses; **TTR-1v′**, purple triangles; **TTR-1vi′**, pink upside down triangles). (B) Plot displaying the extent of tetramer dissociation after 168 h in 6.0 M urea. The shorter linkers demonstrate a large amount of tetramer dissociation, which is drastically reduced as the linker length is increased. The dotted line represents the extent of dissociation for the control heterotetramer ((flag-tag WT TTR)$_1$(C10A)$_3$) in the absence of small molecule. (C) Dissociation kinetics of **TTR-1i′**−**TTR-1vi′** treated with 1 mM DTT in 6.0 M urea. The untethered molecules demonstrate an inverse relationship, relative to the tethered molecules, between their ability to inhibit tetramer dissociation and linker length.

little dissociation over the time course of this experiment (Figure 7B), indicating that occupancy of a single T_4 site by an inhibitor can impose kinetic stabilization on the entire TTR tetramer. Experiments below demonstrate that the small (<20%) dissociation amplitude observed for **TTR-1iii′**−**TTR-1vi′** results from unmodified TTR remaining in solution; hence, it can be

(45) Hammarstrom, P.; Jiang, X.; Hurshman, A. R.; Powers, E. T.; Kelly, J. W. *Proc. Natl. Acad. Sci. U.S.A.* **2002**, *99*, 16427−16432.

concluded that **TTR-1iii′**−**TTR-1vi′** do not dissociate in 6.0 M urea. DTT reduction of **TTR-1i′**−**TTR-1vi′** reveals that the efficacy of the untethered inhibitors is highly dependent on the length of the PEG linker (Figure 7C). Surprisingly, the least effective tethered inhibitors (**TTR-1i′** and **TTR-1ii′**; Figure 7A) proved to be the most effective untethered inhibitors of tetramer dissociation (Figure 7C). This inverse relationship is most likely a result of the length of the PEG linker reducing the binding constants of the free ligands proportional to the number of PEG units.

Sedimentation velocity analytical ultracentrifuge data on a sample of **TTR-1vi′** that had been incubated in 6.0 M urea for 168 h revealed that ~80% of the conjugate was tetrameric and ~20% monomeric (data not shown), indicating that the observed transition in the kinetic urea dissociation experiment is not an artifact (Figure 7A). The dissociation rate constant reflecting the 20% amplitude was determined to be ~0.030 h^{-1} for **TTR-1iii′**−**TTR-1vi′**, a rate very similar to that exhibited by (flag-tag WT)$_1$(C10A)$_3$ TTR. The similarity in rates suggests that the observed dissociation results from the incomplete labeling of the (flag-tag WT)$_1$(C10A)$_3$ TTR heterotetramer. Consistent with this interpretation, a 10−15% amplitude is also observed under acid-mediated amyloidogenesis (Figure 6A). Aggregates from these samples were subjected to centrifugation, isolated, and redissolved in DMSO to determine their composition. HPLC analysis revealed that the aggregates consisted primarily of C10A and unmodified flag-tag WT TTR (Supporting Information Figure 2A), demonstrating that the small amount of aggregation (Figure 6A) and dissociation (Figure 7A) is attributable to a small fraction (<20%) of unmodified (flag-tag WT TTR)$_1$(C10A)$_3$ heterotetetramers.

To provide more evidence to support this hypothesis, **TTR-1iv′** was subjected to acid-mediated aggregation conditions (pH 4.2, 37 °C) for 72 h, centrifuged, and filtered to remove the fraction of unlabeled tetramer capable of aggregating. HPLC, LCMS, and SDS−PAGE confirmed that the supernatant consisted of one flag-tag WT subunit tethered to an inhibitor and three C10A subunits (data not shown). This pretreated protein was subjected to urea denaturation (6.0 M urea) to measure its dissociation kinetics, revealing a dramatic decrease in the amplitude of the dissociation phase (Supporting Information Figure 2B). Collectively these data demonstrate that the unconjugated protein is responsible for the small amplitude observed in the urea-mediated denaturation assay, strongly supporting our conclusion that single inhibitor occupancy is sufficient to impose kinetic stabilization on the native tetrameric structure of TTR.

Discussion

The binding of small molecules to proteins stabilizes the native state proportional to the binding constant. This stabilization not only shifts the equilibrium toward the folded state, but it also can raise the kinetic barrier between the native state and the transition state associated with denaturation, provided that the small molecule stabilizes the native state selectively over the transition state. We previously demonstrated that native state kinetic stabilization is a viable therapeutic approach to prevent TTR amyloidoses.[10] Herein, we show that occupancy of one T_4 binding site within TTR is sufficient to dramatically slow dissociation of the entire TTR tetramer under denaturing conditions (urea and acid). Tethering a small molecule to TTR with an optimal linker length creates a very high local concentration of ligand at the binding site, which results in a high population of a stabilized singly occupied TTR tetramer.

Stabilization of One of the Quaternary Structural Interfaces Associated with Inhibitor Binding Is Sufficient To Impose Kinetic Stabilization on the Entire TTR Tetramer. Herein, we show that occupancy of one T_4 binding site by an aromatic inhibitor facilitates intersubunit hydrophobic contacts that impose kinetic stabilization on the entire TTR tetramer by selective stabilization of the ground state over the dissociation transition state. We recently demonstrated that connecting the C-terminus to the N-terminus on only one of the two pairs of subunits composing the T_4 binding sites can also impose kinetic stabilization on the entire tetramer under denaturing conditions.[46] From the work described herein, and elsewhere,[10,46,47] it would appear that the dissociation of TTR about the T_4 binding site interface is energetically most feasible; thus, stabilization or perturbation of this interface is critical to achieve kinetic stabilization.

Substoichiometric Concentrations of TTR Amyloidogenesis Inhibitors Prevent TTR Amyloidogenesis in Vitro. Substantial inhibition of amyloidogenesis does not require that every TTR tetramer be kinetically stabilized by small molecule binding. Misfolded monomeric TTR aggregates into amyloid via a downhill polymerization mechanism where all forward steps in the pathway are favorable; hence, the rate of aggregation is dependent on the concentration of the misfolded TTR monomer.[18] Since the concentration of monomer is dependent on the dissociation of the tetramer, it is evident that controlling tetramer dissociation energetics will allow significant control over the amyloidogenic monomer concentration, which dictates the rate of TTR amyloidogenesis. Even substoichiometric concentrations (<1 equiv) of small molecule inhibitors may be sufficient to adequately reduce the concentration of monomeric TTR in the serum below the concentration where aggregation is efficient, thereby preventing disease.

The sufficiency of a single binding event to stabilize the entire TTR tetramer suggests that the most efficient molecules for native state stabilization of TTR would display striking negative cooperativity, with a K_{d1} in the nanomolar or subnanomolar range and a K_{d2} in the micromolar (or millimolar) range, maximizing the population of TTR·I. At substoichiometric ligand concentrations positive and noncooperative ligands would bind a lower mole fraction of TTR tetramers monovalently because some tetramers would be doubly liganded and others unliganded as dictated by the two dissociation constants. An ideal inhibitor would display strong negative cooperativity between the two thyroxine binding sites, increasing the total population of bound tetramer ($T{\cdot}I + T{\cdot}I_2$) and lowering the population of unbound tetramer capable of undergoing amyloidogenesis (Figure 8). Ideal molecules would also display high binding selectivity for TTR over other proteins in the serum. High binding selectivity, negative cooperativity, and a subnanomolar K_{d1} would allow inhibitor concentrations equal to or less than the TTR protein concentration to be employed, minimizing pharmaceutical side effects.

(46) Foss, T.; Kelker, M. S.; Wiseman, R. L.; Wilson, I. A.; Kelly, J. W. *J. Mol. Biol.* **2005**, *347*, 841−854.
(47) Schormann, N.; Murrell, J. R.; Benson, M. D. *Amyloid* **1998**, *5*, 175−187.

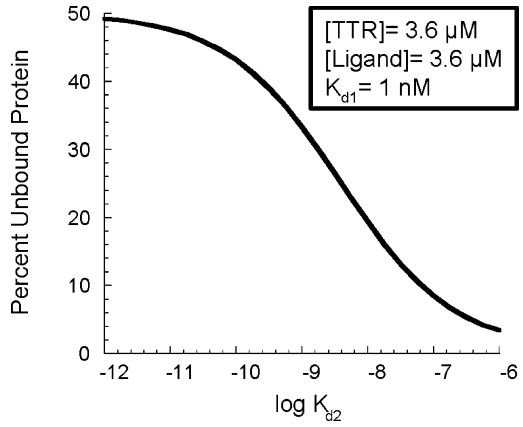

Figure 8. Plot displaying the concentration of unbound protein as a function of the second dissociation constant of a soluble inhibitor (TTR concentration = 3.6 μM, K_{d1} = 1 nM). Increasing K_{d2} decreases the amount of unbound protein, demonstrating that negatively cooperative small molecules appear to be ideal to prevent TTR amyloidogenesis.

Conclusions

Prior to this work it was established that the inhibition of TTR tetramer dissociation, which is rate-limiting for fibril formation, could be mediated by amyloidogenesis inhibitor occupancy of both T_4 binding sites. Using the tethering approach described above it is now safe to conclude that occupancy of a single T_4 binding site is capable of imposing kinetic stabilization on the entire tetrameric structure. Because binding of one T_4 binding site is sufficient to dramatically inhibit amyloidogenesis, it is now evident that the therapeutic concentration of small molecule amyloidogenesis inhibitors could be lowered if a negatively cooperative, TTR-selective small molecule could be discovered that has a nanomolar K_{d1} and a micromolar, or preferably a millimolar, K_{d2}.

Experimental Section

General Synthetic Methods.

Unless otherwise stated, all chemicals were purchased from commercial suppliers and used without further purification. Reaction progress was monitored by thin-layer chromatography on silica gel 60 F254-coated glass plates (EM Sciences) and/or analytical RP-HPLC. All flash chromatography was performed using 230−400 mesh silica gel 60 (EM Sciences). NMR spectra were recorded on either a Bruker 500 or 600 MHz spectrometer. Chemical shifts are reported in parts per million downfield from the internal standard Me_4Si (0.0 ppm) for $CDCl_3$ solutions, or in the case where the Me_4Si was not seen in the ^{13}C NMR spectra, calibration was done on the solvent peaks ($CDCl_3$ 77.16 ppm). For samples in d_6-DMSO, d_6-acetone, or CD_3OD, calibration was done on the solvent peak at 2.49, 2.05, and 3.31 ppm, respectively, for ^1H NMR and 39.52, 29.84, and 49.00 ppm, respectively, for ^{13}C NMR. Reverse-phase high-performance liquid chromatography (RP-HPLC) was carried out on a Waters 600 E multisolvent delivery system employing a Waters 486 tunable absorbance detector and a Waters 717 autosampler. A ThermoHypersil-Keystone Betabasic-18 column was used for analytical reverse-phase HPLC analyses (model 71503-034630, 150 Å pore size, 3 μm particle size). Solvent system A was 95:5 H_2O:CH_3CN with 0.25% trifluoroacetic acid, and solvent B was 5:95 H_2O:CH_3CN with 0.25% trifluoroacetic acid; linear gradients were run from either 0:100, 80:20, or 60:40 A:B to 0:100 A:B. All mass spectrometry data were collected at the Scripps Research Institute Center for Mass Spectrometry.

4-Benzyloxy-3,5-dichloroaniline (3).

Benzyl bromide (3.10 mL, 25.9 mmol) was added slowly to a stirring mixture of potassium carbonate (3.95 g, 28.6 mmol) and 4-amino-2,6-dichlorophenol (5.06 g, 28.4 mmol) in acetone. After stirring for 20 h the reaction was concentrated to a slurry, diluted with water (200 mL), and extracted with EtOAc (3 × 100 mL). The combined organics were washed with saturated $NaHCO_3$ (2 × 25 mL) and brine (25 mL) and extracted with 30% HCl (3 × 30 mL), and the white precipitate was filtered and rinsed with EtOAc. The aqueous layer of the filtrate was separated and washed with dichloromethane (2 × 30 mL), combined with the white precipitate, adjusted to pH ≈ 8 with NaOH pellets, and extracted with DCM (2 × 50 mL). The combined DCM extracts were washed with brine (25 mL), dried over Na_2SO_4, filtered, and concentrated to afford 4-benzyloxy-3,5-dichloroaniline (**3**) as a tan solid (5.01 g, 66%). ^1H NMR (600 MHz, $CDCl_3$) δ 7.53−7.57 (m, 2H), 7.37−7.41 (m, 2H), 7.32−7.36 (m, 1H), 6.60 (s, 2H), 4.94 (s, 2H), 3.62 (s, 2H); ^{13}C NMR (150 MHz, $CDCl_3$) δ 143.68, 143.13, 136.82, 129.93, 128.62, 128.55, 128.39, 115.11, 75.22; ESI-MS 268 *m*/*z* $[MH]^+$, $C_{13}H_{12}Cl_2NO$ requires 268.

Methyl 2-(4-Benzyloxy-3,5-dichlorophenylamino)benzoate (4a).

Toluene (10.0 mL) was added to a flask charged with **3** (1.17 g, 5.36 mmol), methyl 2-bromobenzoate (0.73 mL, 5.20 mmol), tris-(dibenzylideneacetone)dipalladium (0) (183 mg, 0.200 mmol), (*R*)-(+)-2,2′-bis(diphenylphosphino)-1,1′-binaphthyl (82.4 mg, 0.132 mmol), and cesium carbonate (2.00 g, 6.14 mmol) and then stirred at reflux under an argon atmosphere. After 24 h the reaction was filtered through Celite and concentrated. Flash chromatographic purification over silica (9:1−4:1 hexanes:EtOAc gradient elution) afforded methyl 2-(4-benzyloxy-3,5-dichlorophenylamino)benzoate (**4a**) as a yellow solid (1.20 g, 68%). ^1H NMR (500 MHz, $CDCl_3$) δ 9.44 (s, 1H), 7.98 (dd, J = 1.7, 8.0 Hz, 1H), 7.56−7.59 (m, 2H), 7.34−7.43 (m, 2H), 7.33−7.38 (m, 2H), 7.23 (apparent dd, J = 0.8, 8.5 Hz, 1H), 7.21 (s, 2H), 6.82 (apparent ddd, J = 1.1, 7.0, 8.0 Hz, 1H), 5.03 (s, 2H), 3.90 (s, 3H); ^{13}C NMR (125 MHz, $CDCl_3$) δ 168.95, 146.88, 146.84, 138.32, 136.58, 134.47, 131.91, 130.22, 128.67, 128.62, 128.54, 122.17, 118.52, 114.59, 113.06, 75.27, 52.10; ESI-MS 402 *m*/*z* $[MH]^+$, $C_{21}H_{18}Cl_2NO_3$ requires 402, 424 *m*/*z* $[MNa]^+$, $C_{21}H_{17}Cl_2NaNO_3$ requires 424.

Methyl 2-(4-Hydroxy-3,5-dichlorophenylamino)benzoate (4b).

Ten percent palladium on carbon (64.3 mg, 0.0604 mmol) and **4a** (1.90 g, 4.72 mmol) were stirred in a 1:1 mixture of MeOH:EtOAc (48 mL) under a hydrogen atmosphere for 6 h. The atmosphere was then purged with argon, and the reaction was quenched with DCM, filtered through Celite, and concentrated, affording methyl 2-(4-hydroxy-3,5-dichlorophenylamino)benzoate (**4b**) as a greenish solid (1.42 g, 97%). ^1H NMR (500 MHz, d_6-DMSO) δ 9.93 (s, 1H), 9.06 (s, 1H), 7.86 (dd, J = 1.6, 8.0 Hz, 1H), 7.40 (apparent ddd, J = 1.6, 7.1, 8.5 Hz, 1H), 7.26 (s, 2H), 7.02 (apparent dd, J = 0.7, 8.5 Hz, 1H), 6.79 (apparent ddd, J = 0.9, 7.1, 8.0 Hz, 1H), 3.83 (s, 3H); ^{13}C NMR (125 MHz, d_6-DMSO) δ 167.84, 147.04, 145.55, 134.60, 133.50, 131.32, 123.23, 122.86, 117.81, 114.17, 112.08, 51.99; ESI-MS 312 *m*/*z* $[MH]^+$, $C_{14}H_{12}Cl_2NO_3$ requires 312.

Methyl 2-(4-Methoxy-3,5-dichlorophenylamino)benzoate (4c).

Methyliodide (25.0 μL, 0.40 mmol), methyl 2-(4-hydroxy-3,5-dichlorophenylamino)benzoate (**4b**) (103.0 mg, 0.330 mmol), and K_2CO_3 (50.9 mg, 0.368 mmol) were stirred in anhydrous DMF under an argon atmosphere for 18 h. The reaction was then poured into water (35 mL) and extracted with EtOAc (3 × 20 mL). The combined organics were washed with water (3 × 30 mL), dried over Na_2SO_4, filtered, and concentrated. Flash chromatographic purification over silica (4:1 hexanes:EtOAc) afforded methyl 2-(4-methoxy-3,5-dichlorophenylamino)benzoate (**4c**) as a white solid (79.1 mg, 73%). ^1H NMR (500 MHz, $CDCl_3$) δ 9.42 (s, 1H), 7.97 (dd, J = 1.4, 8.0 Hz, 1H), 7.38 (apparent ddd, J = 1.3, 7.1, 8.4 Hz, 1H), 7.21 (d, J = 8.6 Hz, 1H), 7.19 (s, 2H), 6.81 (apparent ddd, J = 0.8, 7.2, 8.0 Hz, 1H), 3.90 (s, 3H), 3.89 (s, 3H); ^{13}C NMR (125 MHz, $CDCl_3$) δ 168.93, 148.15, 146.88, 138.11, 134.46, 131.88, 129.85, 122.25, 118.44, 114.48, 112.93, 61.00, 52.10; ESI-MS 326 *m*/*z* $[MH]^+$, $C_{15}H_{14}Cl_2NO_3$ requires 326.

Representative Procedure for the Mitsunobu Coupling of Monomethyl Poly(ethylene glycol)s to Methyl 2-(4-Hydroxy-3,5-dichlorophenylamino)benzoate (4b). *Synthesis of Methyl 2-(3,5-Dichloro-4-(2-methoxyethoxy)phenylamino)benzoate (**4d**)*.

Diisopropyl azodicarboxylate (40.0 μL, 0.202 mmol) was added dropwise to a stirring solution of 2-(4-hydroxy-3,5-dichlorophenylamino)benzoate (**4b**) (63.0 mg, 0.202 mmol), 2-methoxyethanol (16.0 μL, 0.203 mmol), and triphenylphosphine (58.5 mg, 0.223 mmol) in anhydrous THF (2.0 mL) under an argon atmosphere. After 24 h the reaction was concentrated, and flash chromatographic purification over silica (9:1−2:1 hexanes:EtOAc gradient elution) afforded **4d** as a pale yellow syrup (66.2 mg, 89%). ^{1}H NMR (500 MHz, $CDCl_3$) δ 9.42 (s, 1H), 7.97 (dd, J = 1.6, 8.0 Hz, 1H), 7.38 (apparent ddd, J = 1.6, 7.1, 8.5 Hz, 1H), 7.21 (dd, J = 0.7, 8.5 Hz, 1H), 7.18, (s, 2H), 6.81 (apparent ddd, J = 1.0, 7.1, 8.0 Hz, 1H), 4.16−4.19 (m, 2H), 3.90 (s, 3H), 3.79−3.82 (m, 2H), 3.48 (s, 3H); ^{13}C NMR (125 MHz, $CDCl_3$) δ 168.92, 147.21, 146.82, 138.13, 134.45, 131.88, 129.88, 122.11, 118.46, 114.54, 112.97, 72.67, 71.72, 59.32, 52.10; ESI-MS 370 *m*/*z* $[MH]^+$, $C_{17}H_{18}Cl_2NO_4$ requires 370, 392 *m*/*z* $[MNa]^+$, $C_{17}H_{17}Cl_2NaNO_4$ requires 392.

Mitsunobu procedures and characterization data for compounds **4e** and **4f** are presented in the Supporting Information.

Representative Procedure for the Hydrolysis of Methyl Esters 4a−f. *Synthesis of 2-(3,5-Dichloro-4-benzyloxyphenylamino)benzoic Acid (5a).*

$LiOH\cdot H_2O$ (1.33 g, 31.7 mmol) was added to a stirring solution of **4a** (3.16 g, 7.86 mmol) in THF:MeOH:H_2O (18:6:6 mL). After 18 h the reaction was diluted with H_2O (200 mL) and acidified to pH $\approx$ 1 with 30% HCl, whereupon the precipitate was filtered, washed with H_2O, collected, and dried to yield **5a** as a pale yellow powder (3.05 g, 100%). ^{1}H NMR (500 MHz, d_6-DMSO) δ 9.52 (br s, 1H), 7.91 (dd, J = 1.7, 8.0 Hz, 1H), 7.51−7.54 (m, 2H), 7.36−7.48 (m, 6H), 7.23 (dd, J = 0.7, 8.3 Hz, 1H), 6.88 (apparent ddd, J = 0.9, 7.1, 8.0 Hz, 1H), 4.97 (s, 2H); ^{13}C NMR (125 MHz, d_6-DMSO) δ 169.53, 145.42, 145.18, 138.82, 136.24, 134.25, 131.89, 129.09, 128.45, 128.42, 128.39, 120.71, 119.01, 115.20, 114.48, 74.79; ESI-MS 388 *m*/*z* $[MH]^+$, $C_{20}H_{16}Cl_2NO_3$ requires 388, 410 *m*/*z* $[MNa]^+$, $C_{20}H_{15}Cl_2NaNO_3$ requires 410.

Hydrolysis procedures and characterization data for compounds **5b−f** are presented in the Supporting Information.

Representative Procedure for the Monoprotection of Poly(ethylene glycol)s. *Synthesis of Ethylene Glycol Monobenzoate (6i).*

Benzoyl chloride (2.90 mL, 25.0 mmol) was added slowly to a stirring solution of ethylene glycol (4.20 mL, 75.3 mmol) and pyridine (2.25 mL, 27.6 mmol) in 25 mL of anhydrous dichloromethane (DCM) at 0 °C under an argon atmosphere. After stirring for an additional 24 h at room temperature the reaction was then diluted with ethyl acetate (200 mL), washed with water (3 × 50 mL) and brine (50 mL), dried over Na_2SO_4, filtered, and concentrated. Flash chromatographic purification over silica (2:1−1:1 hexanes:EtOAc gradient elution) afforded ethylene glycol monobenzoate (**6i**) as a clear, colorless liquid (3.30 g, 79%). ^{1}H NMR (500 MHz, $CDCl_3$) δ 8.04−8.08 (m, 2H), 7.55−7.60 (m, 1H), 7.42−7.47 (m, 2H), 4.45−4.48 (m, 2H), 3.96 (br s, 2H), 2.31 (br s, 1H); ^{13}C NMR (125 MHz, $CDCl_3$) δ 166.99, 133.20, 129.84, 129.69, 128.42, 66.67, 61.38.

Monoprotection procedures and characterization data for compounds **6ii−vi** are presented in the Supporting Information.

Representative Procedure for the Bromination of Poly(ethylene glycol) Monobenzoates. *Synthesis of Bromoethylene Glycol Benzoate (7i).*

Triphenylphosphine (5.99 g, 22.8 mmol in 45 mL of anhydrous DCM) was added slowly to a stirring solution of *N*-bromosuccinimide (4.05 g, 22.8 mmol in 100 mL of anhydrous DCM) at −78 °C under an argon atmosphere. After 10 min the **6i** (3.16 g, 19.0 mmol in 45 mL of anhydrous DCM) was added slowly, and then the reaction was left stir while warming to room temperature. After 2 h the reaction was concentrated with silica to a powder. Flash chromatographic purification over silica (4:1 hexanes:EtOAc) afforded bromoethylene glycol benzoate (**7i**) as a clear, pale yellow liquid (4.30 g, 99%). ^{1}H NMR (500 MHz, $CDCl_3$) δ 8.06−8.09 (m, 2H), 7.58 (apparent tt, J = 1.4, 7.5 Hz, 1H), 7.44−7.48 (m, 2H), 4.63 (t, J = 6.1 Hz, 2H), 3.65 (t, J = 6.1 Hz, 2H); ^{13}C NMR (125 MHz, $CDCl_3$) δ 166.08, 133.29, 129.75, 129.61, 128.46, 64.21, 28.80.

Bromination procedures and characterization data for compounds **7ii−vi** are presented in the Supporting Information.

Representative Procedure for the Nucleophilic Coupling of Thioacetic Acid to Bromopoly(ethylene glycol) Benzoates. *Synthesis of Acetylsulfanylethylene Glycol Benzoate (8i).*

Thioacetic acid (75.0 μL, 1.05 mmol) was added to a stirring solution of sodium hydride (41.8 mg, 1.05 mmol) in anhydrous DMF (5 mL) under an argon atmosphere. After 30 min the **7i** (219.2 mg, 0.957 mmol in 5 mL of anhydrous DMF) was added, the reaction was stirred for 30 min, and then diluted with EtOAc (100 mL), washed with water (3 × 25 mL) and brine (25 mL), dried over Na_2SO_4, filtered, and concentrated. Flash chromatographic purification over silica (9:1 hexanes:EtOAc) afforded acetylsulfanylethylene glycol benzoate (**8i**) as a clear, colorless liquid (161.2 mg, 75%). ^{1}H NMR (500 MHz, $CDCl_3$) δ 8.02−8.05 (m, 2H), 7.57 (tt, J = 1.5, 7.5 Hz, 1H), 7.43−7.47 (m, 2H), 4.43 (t, J = 6.4 Hz, 2H), 3.28 (t, J = 6.4 Hz, 2H), 2.37 (s, 3H); ^{13}C NMR (125 MHz, $CDCl_3$) δ 195.05, 166.35, 133.25, 129.94, 129.78, 128.53, 63.33, 30.69, 28.10; ESI-MS 247 *m*/*z* $[MNa]^+$, $C_{11}H_{12}NaO_3S$ requires 247.

Thioacetic acid nucleophilic substitution procedures and characterization data for compounds **8ii−vi** are presented in the Supporting Information.

Representative Procedure for the Deprotection of Acetylsulfanylpoly(ethylene glycol) Benzoates and Masking of Thiols as 2-Mercaptopyridine Disulfides. *Synthesis of Masked Thiol 9i.*

Sodium methoxide (1.40 mL of 0.5 M in MeOH, 0.70 mmol) was added dropwise to a stirring solution of **8i** (70.9 mg, 0.316 mmol) and 2,2′-dithiodipyridine (77.4 mg, 0.351 mmol) in anhydrous methanol (3 mL) under an argon atmosphere. After 2 h the reaction was concentrated with silica to a powder, and the crude product was purified by flash chromatography over silica (1:1 hexanes:EtOAc) to afford **9i** as a clear, pale yellow liquid (26.3 mg, 44%). Alternatively, 2,2′-dithiodipyridine (2.03 g, 9.21 mmol) was added to a stirring solution of 2-mercaptoethanol (0.65 mL, 9.2 mmol) in anhydrous methanol (90 mL) under an argon atmosphere. After 1 h the reaction was concentrated with silica to a powder, and the crude product was purified by flash chromatography over silica (1:1 hexanes:EtOAc) to afford **9i** as a clear, pale yellow liquid (1.15 g mg, 67%). ^{1}H NMR (500 MHz, $CDCl_3$) δ 8.51 (ddd, J = 0.9, 1.8, 5.0 Hz, 1H), 7.59 (apparent dt, J = 1.8, 7.7 Hz, 1H), 7.41 (dt, J = 0.9, 8.1 Hz, 1H), 7.16 (ddd, J = 0.9, 5.0, 7.3 Hz, 1H), 5.75 (t, J = 7.0 Hz, 1H), 3.78−3.83 (m, 2H), 2.94−2.98 (m, 2H); ^{13}C NMR (125 MHz, $CDCl_3$) δ 159.21, 149.97, 136.97, 122.06, 121.64, 58.32, 42.80; ESI-MS 188 *m*/*z* $[MH]^+$, $C_7H_{10}OS_2$ requires 188, 210 *m*/*z* $[MNa]^+$, $C_7H_9NaOS_2$ requires 210.

2-Mercaptopyridine disulfide protection procedures and characterization data for compounds **9ii−vi** are presented in the Supporting Information.

***tert*-Butyl 2-Bromobenzoate (10).**

tert-Butyl alcohol (1.80 g, 24.2 mmol) in anhydrous dichloromethane (10 mL) was added to a stirring mixture of 2-bromobenzoic acid (2.02 g, 10.0 mmol), *N*,*N*′-dicyclohexylcarbodiimide (2.49 g, 12.1 mmol), and *N*,*N*-(dimethylamino)pyridine (123 mg, 1.01 mmol) in anhydrous dichloromethane (40 mL) under an argon atmosphere. After stirring for 24 h the reaction was concentrated and chromatographed over silica (9:1−4:1 hexanes:EtOAc gradient elution), affording *tert*-butyl 2-bromobenzoate **(10)** as a clear, colorless liquid (1.57 g, 61%). ^{1}H NMR (500 MHz, $CDCl_3$) δ 7.68 (dd, J = 1.8, 7.6 Hz, 1H), 7.61 (dd, J = 1.2, 7.9 Hz, 1H), 7.33 (dt, J = 1.2, 7.6 Hz, 1H), 7.27 (dt, J = 1.8, 7.9 Hz), 1.61 (s, 9H); ^{13}C NMR (125 MHz, $CDCl_3$) δ 165.83, 134.43, 134.14, 131.97, 130.92, 127.20, 121.10, 82.68, 28.26; GC-MS 256/258 *m*/*z* $[M]^+$, $C_{11}H_{13}BrO_2$ requires 256/258, 183/185 *m*/*z* $[M - C_4H_9O]^+$, C_7H_4BrO requires 183/185.

***tert*-Butyl 2-(4-Benzyloxy-3,5-dichlorophenylamino)benzoate (11).**

Toluene (11.0 mL) was added to a flask charged with **10** (1.76 g, 6.56 mmol), **3** (1.40 g, 5.44 mmol), tris(dibenzylideneacetone)-dipalladium(0) (533 mg, 0.857 mmol), (*R*)-(+)-2,2′-bis)diphenylphosphino)-1,1′-binaphthyl (109 mg, 0.175 mmol), and cesium carbonate

(2.48 g, 7.61 mmol) and then stirred at reflux under an argon atmosphere. After 24 h the reaction was filtered through Celite and concentrated. Flash chromatographic purification over silica (95:5 hexanes:EtOAc) afforded *tert*-butyl 2-(4-benzyloxy-3,5-dichlorophenylamino)benzoate (**11**) as a pale yellow solid (1.40 g, 58%). ^{1}H NMR (600 MHz, $CDCl_3$) δ 9.57 (s, 1H), 7.93 (dd, J = 1.6, 8.0 Hz, 1H), 7.57 (apparent d, J = 7.6 Hz, 2H), 7.39−7.43 (m, 2H), 7.33−7.38 (m, 2H), 7.23 (apparent d, J = 8.4 Hz, 1H), 7.21 (s, 2H), 6.78−6.82 (m, 1H), 5.02 (s, 2H), 1.60 (s, 9H); ^{13}C NMR (150 MHz, $CDCl_3$) δ 168.04, 146.61, 146.50, 138.58, 136.58, 133.91, 132.11, 130.12, 128.67, 128.62, 128.52, 121.72, 118.38, 114.75, 114.57, 81.78, 75.24, 28.42; ESI-MS 478 *m*/*z* $[M + Cl]^-$, $C_{24}H_{23}Cl_3NO_3$ requires 478.

***tert*-Butyl 2-(4-Hydroxy-3,5-dichlorophenylamino)benzoate (12).** Ten percent palladium on carbon (158 mg, 0.148 mmol) and **11** (1.32 g, 2.97 mmol) were stirred in a 1:1 mixture of MeOH:EtOAc (16 mL) under a hydrogen atmosphere for 5 h. The atmosphere was then purged with argon, and the reaction was quenched with DCM, filtered through Celite, and concentrated. Flash chromatographic purification over silica (9:1−4:1 hexanes:EtOAc gradient elution) afforded *tert*-butyl 2-(4-hydroxy-3,5-dichlorophenylamino)benzoate (**12**) as a pale yellow solid (932 mg, 89%). ^{1}H NMR (500 MHz, $CDCl_3$) δ 9.44 (s, 1H), 7.91 (dd, J = 1.6, 8.0 Hz, 1H), 7.31 (apparent ddd, J = 1.6, 7.1, 8.5 Hz, 1H), 7.24 (s, 2H), 7.05 (dd, J = 0.8, 8.5 Hz, 1H), 6.74 (apparent ddd, J = 0.9, 7.2, 8.0 Hz, 1H), 5.67 (s, 1H), 1.60 (s, 9H); ^{13}C NMR (125 MHz, $CDCl_3$) δ 168.15, 147.85, 144.37, 134.68, 133.96, 132.06, 123.39, 121.43, 117.60, 113.84, 113.79, 81.61, 28.44; ESI-MS 354 *m*/*z* $[MH]^+$, $C_{17}H_{18}Cl_2NO_3$ requires 354, 376 *m*/*z* $[MNa]^+$, $C_{17}H_{17}Cl_2NaNO_3$ requires 376.

Representative Procedure for the Mitsunobu Coupling of Activated Thiol Linkers to *tert*-Butyl 2-(4-Hydroxy-3,5-dichlorophenylamino)benzoate (12). *Synthesis of **13i**.*

Diisopropyl azodicarboxylate (58.0 μL, 0.293 mmol) was added dropwise to a stirring solution of triphenylphosphine (76.6 mg, 0.292 mmol) in anhydrous THF (5.0 mL) under an argon atmosphere. After 30 min **9i** (54.5 mg, 0.291 mmol) and **12** (51.7 mg, 0.146 mmol) in anhydrous THF (5.0 mL) were added to the DIAD/PPh_3 mixture, and the reaction was stirred for 1 h and then concentrated. Flash chromatographic purification over silica (9:1−4:1 hexanes:EtOAc gradient elution) afforded **13i** as a clear, colorless syrup (69.9 mg, 91%). ^{1}H NMR (500 MHz, $CDCl_3$) δ 9.55 (s, 1H), 8.48 (ddd, J = 0.7, 1.7, 4.8 Hz, 1H), 7.92 (dd, J = 1.6, 8.0 Hz, 1H), 7.77 (apparent dt, J = 1.0, 8.1 Hz, 1H), 7.66 (ddd, J = 1.8, 7.4, 8.0 Hz, 1H), 7.35 (apparent ddd, J = 1.6, 7.1, 8.5 Hz, 1H), 7.22 (dd, J = 0.9, 8.5 Hz, 1H), 7.17 (s, 2H), 7.10 (ddd, J = 1.0, 4.8, 7.4 Hz, 1H), 6.80 (apparent ddd, J = 0.9, 7.2, 8.0 Hz, 1H), 4.29 (t, J = 6.7 Hz, 2H), 3.25 (t, J = 6.7 Hz, 2H), 1.60 (s, 9H); ^{13}C NMR (125 MHz, $CDCl_3$) δ 168.01, 160.07, 149.85, 146.51, 146.45, 138.64, 137.26, 133.91, 132.11, 129.75, 121.60, 120.91, 119.99, 118.45, 114.82, 114.60, 81.82, 71.61, 38.50, 28.42; ESI-MS 523 *m*/*z* $[MH]^+$, $C_{24}H_{25}Cl_2N_2O_3S_2$ requires 523.

Mitsunobu procedures and characterization data for compounds **13ii**−**vi** are presented in the Supporting Information.

Representative Procedure for the Deprotection of *tert*-Butyl Esters 13i−vi. *Synthesis of **1i**.*

Compound **13i** (62.9 mg, 0.120 mmol) was stirred in trifluoroacetic acid (5.0 mL) for 3 h, and then it was concentrated, diluted with water, and lyophilized to afford **1i** as a grayish solid in quantitative yield. ^{1}H NMR (600 MHz, d_6-DMSO) δ 13.20 (br s, 1H), 9.48 (s, 1H), 8.45−8.47 (m, 1H), 7.90 (dd, J = 1.6, 7.9 Hz, 1H), 7.78−7.85 (m, 2H), 7.45 (apparent ddd, J = 1.6, 7.1, 8.4 Hz, 1H), 7.33 (s, 2H), 7.23−7.26 (m, 2H), 6.86−6.90 (m, 1H), 4.21 (t, J = 6.2 Hz, 2H), 3.26 (t, J = 6.2 Hz, 2H); ^{13}C NMR (150 MHz, d_6-DMSO) δ 169.50, 158.86, 149.66, 145.36, 145.17, 138.83, 137.87, 134.24, 131.86, 128.73, 121.34, 120.63, 119.50, 119.03, 115.25, 114.48, 71.22, 38.00; MALDI−FTMS (DHB) 467.0049 *m*/*z* $[MH]^+$, $C_{20}H_{17}Cl_2N_2O_3S_2$ requires 467.0052.

tert-Butyl deprotection procedures and characterization data for compounds **1ii**−**vi** are presented in the Supporting Information.

Expression and Purification of (flag-tag WT TTR)$_1$(C10A)$_3$. C10A TTR and flag-tag WT TTR were co-transformed into BL21 (DE3) Epicurian Gold cells (Stratagene) with both the C10A TTR/pMMHa and the flag-tag WT TTR/pet29a expression vectors. Selection was performed by overnight growth (37 °C) on agar plates containing 150 μg/mL kanamycin and 100 μg/mL ampicillin. Starter cultures were prepared by the inoculation of LB media (150 μg/mL kanamycin, 100 μg/mL ampicillin) with a single colony from the agar plate. Starter cultures were grown at 37 °C, with shaking, until bacteria growth was observed. Expression cultures (LB media with 150 μg/mL kanamycin and 100 μg/mL ampicillin) were then inoculated with a 1:100 dilution of the starter cultures, grown at 37 °C until $OD_{600} \approx 0.8$, and induced by addition of 1 mM IPTG. Induction was allowed to proceed overnight at 37 °C with shaking. Cells were then harvested by centrifugation (14 000*g*, 10 min), resuspended in water, frozen at −80 °C (1 h), and thawed at 37 °C (1 h). Lysates were prepared by sonication (three cycles of 3 min) at 4 °C. Cell debris was pelleted by centrifugation for 30 min at 15 000*g*. The lysate was fractionated by ammonium sulfate precipitation, collecting the pellet of the 50−90% precipitation. This pellet was resuspended in a minimum amount of 25 mM Tris, pH 8.0, 1 mM EDTA and dialyzed overnight (4 °C) against 25 mM Tris, pH 8.0, 1 mM EDTA using 7000 MWCO dialysis tubing (Snakeskin from Pierce Biomedical). The dialysis product was then purified using a Source 15Q anion-exchange column (Amersham Biosciences) running a linear gradient from 200 to 450 mM NaCl in 25 mM Tris, pH 8.0, 1 mM EDTA. Fractions containing the various stoichiometries of C10A and flag-tag WT TTR were pooled and concentrated. The samples were then purified by gel filtration chromatography with a Superdex 75 column (Amersham Biosciences), eluting the sample with 10 mM sodium phosphate (pH 7.2), 100 mM KCl, 1 mM EDTA. The tetrameric peak was collected, and the (flag-tag WT TTR)$_1$(C10A)$_3$ was isolated from other stoichiometries by anion-exchange chromatography with a Source 15Q column (Amersham Biosciences) using the same gradient as above. Protein concentration of (flag-tag WT TTR)$_1$(C10A)$_3$ was determined using the molar absorptivity of $\epsilon = 75\,829\ M^{-1}\ cm^{-1}$. The purified heterotetramer was then stored at 37 °C until modification with small molecule.

Modification of (flag-tag WT TTR)$_1$(C10A)$_3$ with Activated Small Molecules. (flag-tag WT TTR)$_1$(C10A)$_3$ purified above was treated with either 10× activated small molecule (prepared as 10 mM Stock in DMSO) or DMSO for 2 h at room temperature with gentle agitation. The samples were then purified from free small molecules by gel filtration using a Superdex 200 column (Amersham Biosciences) eluting the protein with 10 mM sodium phosphate (pH 7.2), 100 mM KCl, 1 mM EDTA. Purified samples were analyzed with a Waters HPLC using a C8 column (Western Analytical Products, Inc.; 30 × 4.6 mm, 3 μm particle size, and 150 Å pore size) using a linear gradient from 45% to 95% acetonitrile in the presence and absence of 1 mM dithiothreitol (DTT) to ensure modification. LC-ESI-MS (Hewlett-Packard 1100-MSD mass spectrometer) analysis was also performed running a gradient of 15−75% acetonitrile over 10 min, demonstrating that only the flag-tag WT TTR peak was modified by disulfide formation (C10A, 13 860 ± 1 kDa; flag-tag WT TTR, 15 880 ± 1 kDa; **TTR-1i′**, 16 237 ± 1 kDa; **TTR-1ii′**, 16 281 ± 1 kDa; **TTR-1iii′**, 16 325 ± 1 kDa; **TTR-1iv′**, 16 369 ± 1 kDa; **TTR-1v′**, 16 413 ± 1 kDa; **TTR-1vi′**, 16 457 ± 1 kDa). The molar absorptivity of the modified protein was calculated by determining the concentration of the C10A peak on the HPLC trace. The concentration of C10A was determined upon comparison with a standard curve. Because the stoichiometry of C10A to modified flag-tag WT TTR subunits is known, the molar absorptivity can be calculated from the A_{280} of the stock solution of modified protein.

Structural Analysis of Modified Heterotetramers. The tertiary structure of the modified heterotetramers was analyzed using an Aviv model 202SF circular dichroism (CD) spectrometer. The modified heterotetramers (1.8 μM tetramer; 10 mM sodium phosphate

pH 7.2, 100 mM KCl, 1 mM EDTA) in a 2 mm cuvette were scanned from 250 to 200 nm (0.5 nm intervals; 25 °C; 2 s averaging time) averaging five sequential scans to determine the final CD plot.

The quaternary structure of the modified heterotetramers was analyzed using analytical ultracentrifugation. Analytical ultracentrifugation was performed on a Beckman XL-I analytical ultracentrifuge using both interference and absorbance optics. AUC cells were constructed with sapphire windows, 1.2 mm charcoal-filled Epon centerpieces, and used with either an An60 Ti four-hole or an An50 Ti eight-hole rotor. Samples for velocity experiments were allowed to equilibrate to 20 °C for at least 1 h prior to being spun at 50 000 rpm for 4 h, recording absorbance and interference spectra as quickly as instrumentation allowed (ca. every 2−10 min). Scans were analyzed using the c(s) method in SedFit.[48]

Crystallization and Structure Determination of TTR-1iv′.

TTR-1iv′ (6.0 mg mL^{-1}) was crystallized in 3 days from 20% PEG 4K and 0.2 M $CaCl_2 \cdot 2H_2O$ at room temperature using the sitting-drop vapor diffusion method. Crystals were harvested from drops with nylon cryoloops (Hampton Research) and directly cryocooled to −180 °C in cryoprotectant that consisted of well buffer and glycerol (25%). A 1.69 Å native data set was collected on a single crystal at beamline 9-1 at the Stanford Synchrotron Radiation Laboratory (SSRL) in Menlo Park, CA (Table 2). Data were processed and scaled in HKL2000.[49] The space group is orthorhombic $P2_12_12$ with unit cell dimensions $a = 43.65$ Å, $b = 86.64$ Å, and $c = 63.93$ Å and two monomers per asymmetric unit ($V_m = 2.27$ Å^3/Da) with a solvent content of 45.8%.

Diffraction data collected in this experiment were isomorphous with those of a previous structural study of transthyretin (pdb code 1BZD.pdb). [33] An initial model was generated by performing a rigid body refinement and simulated annealing (30−4.00 Å) (starting $R_{cryst} = 55.1\%$, $R_{free} = 46.5\%$; final $R_{cryst} = 32.7\%$, $R_{free} = 33.8\%$) in CNS [50] using the previous model (1BZD.pdb) against the native data. Initial electron density maps were of excellent quality. Refinement to 1.69 Å was performed in CNS.[50] The model was further rebuilt into σ_A-weighted $3F_o - 2F_c$ and $F_o - F_c$ electron density maps in O.[51] Water molecules were assigned automatically in CNS [50] at $>3\sigma$ $F_o - F_c$ difference density peaks and verified by manual inspection in O.[51] After convergence in CNS ($R_{cryst} = 24.6\%$, $R_{free} = 26.3\%$), TLS refinement was continued with REFMAC5[52] with riding hydrogens included. Care was taken to keep the test set intact during all refinement steps. The energy-minimized ligand **1iv′** was built with InsightII (Molecular Simulations, Inc.) and unambiguously placed in the electron density. Both symmetry-related binding conformations of the ligand were in good agreement with unbiased $3F_o - 2F_c$ simulated annealing-omit maps calculated in the absence of the inhibitor. The final model ($R_{cryst} = 21.7\%$, $R_{free} = 23.9\%$; Table 1) is composed of all residues except the first nine and last three of the wild-type sequence and the 16-residue purification tag attached to one monomer, which showed no interpretable electron density, and includes 107 water molecules. The quality of the model was analyzed using the programs Mol Probity,[53] WHAT IF,[54] and PROCHECK.[55] Figure 5 was made using bobscript[56] and raster 3D.[57]

Coordinates and structure factors have been deposited in the Protein Data Bank under the accession code 1U21.

Acid-Induced Aggregation of WT TTR Treated with Compounds 5a−f.

WT TTR (7.2 μM; 10 mM sodium phosphate, pH 7.2, 100 mM KCl, 1 mM EDTA) was incubated with small molecules **5a**−**f** (14.4 μM tetramer) for 30 min at room temperature. The protein samples were diluted 1:1 with acidification buffer containing 100 mM sodium acetate (pH 4.2), 100 mM KCl, 1 mM EDTA. Acidified samples were incubated at 37 °C for 72 h without stirring. The amount of aggregation was analyzed by turbidity measurements (25 °C) at 400 nm on a Hewlett-Packard 8453 UV−visible spectrometer equipped with a Peltier temperature-controlled cell holder.

Acid-Mediated Aggregation of Modified Heterotetramers.

Heterotetramers (7.2 μM; 10 mM sodium phosphate, pH 7.2, 100 mM KCl, 1 mM EDTA) were diluted 1:1 in acidification buffers (pH 3.2−3.6 100 mM sodium citrate, 100 mM KCl, 1 mM EDTA; pH 4.0−5.6 100 mM sodium acetate, 100 mM KCl, 1 mM EDTA; pH 6.0−6.4 100 mM sodium phosphate, 100 mM KCl, 1 mM EDTA). Samples were incubated at 37 °C for 72 h. The extent of aggregation was measured by turbidity at 400 nm on an HP 8453 UV−visible spectrometer equipped with a Peltier temperature-controlled cell holder. Reduced samples were prepared by addition of 1 mM DTT to heterotetrameric samples diluted 1:1 into 100 mM sodium acetate (pH 4.2), 100 mM KCl, 1 mM EDTA and treated as above.

Kinetic Urea Denaturation of Modified Heterotetramers.

Modified heterotetramers (7.2 μM tetramer) were diluted 1:4 with 10 M urea (50 mM sodium phosphate, 100 mM KCl, 1 mM EDTA) and buffer (50 mM sodium phosphate, 100 mM KCl, 1 mM EDTA) to a final solution of 1.8 μM tetrameric protein and 6.0 M urea. Samples were mixed and then immediately measured on an Aviv model 202SF circular dichroism (CD) spectrometer measuring the CD signal at 215 nm (5.0 s averaging time). The samples were incubated at 25 °C, taking CD measurements at the indicated time points. Plots were prepared using Kaleidograph fitting the denaturation to a first-order exponential function with the equation $I = I_o + A(1 - e^{-kt})$, where I = CD signal, I_o = initial CD signal, A = amplitude, k = dissociation rate constant, and t = time. Reduced samples were prepared by the addition of 1 mM DTT to the initial sample preparation and treated as above.

Acknowledgment. This work was supported in part by NIH Grants DK46335 (J.W.K.) and CA58896 and AI42266 (I.A.W.), the Skaggs Institute for Chemical Biology, the Lita Annenberg Hazen Foundation (J.W.K.), an NIH predoctoral training grant T32 AI077606, a Skaggs predoctoral fellowship, David and Ursula Fairchild Fellowship (T.F.), the Jairo H. Arévalo Fellowship (M.S.K.), the Norton B. Gilula Fellowship, and the Fletcher Jones Fellowship (R.L.W.). We thank Dr. L. Xhu for data collection and the SSRL staff of beamline 9.0.1 for guidance during data collection. We thank Drs. Evan T. Powers and Patrick Braun for helpful discussions.

Supporting Information Available: Detailed synthesis and characterization of compounds **1**−**13**, representative sedimentation velocity analytical ultracentrifuge trace of modified (flag-tag WT)$_1$(C10A)$_3$ (**TTR-1iv′**), HPLC traces of redissolved pellets collected from treatment of **TTR-1v′** in acid (pH 4.0, 72 h, 37 °C), and kinetic dissociation plot of **TTR-1iv′** with and without an acid pretreatment (pH 4.2, 72 h, 37 °C). This material is available free of charge via the Internet at http://pubs.acs.org.

JA042929F

(48) Schuck, P. *Biophys. J.* **2000**, *78*, 1606−1619.
(49) Otwinowski, Z.; Minor, W. *Methods Enzymol.* **1997**, *276*, 307−326.
(50) Brunger, A. T.; Adams, P. D.; Clore, G. M.; DeLano, W. L.; Gros, P.; Grosse-Kunstleve, R. W.; Jiang, J. S.; Kuszewski, J.; Nilges, M.; Pannu, N. S.; Read, R. J.; Rice, L. M.; Simonson, T.; Warren, G. L. *Acta Crystallogr., D.: Biol. Crystallogr.* **1998**, *54* (Pt 5), 905−921.
(51) Jones, T. A.; Zou, J. Y.; Cowan, S. W.; Kjeldgaard *Acta Crystallogr., A* **1991**, *47* (Pt 2), 110−119.
(52) Winn, M. D.; Isupov, M. N.; Murshudov, G. N. *Acta Crystallogr., D: Biol. Crystallogr.* **2001**, *57*, 122−133.
(53) Lovell, S. C.; Davis, I. W.; Arendall, W. B., III; de Bakker, P. I.; Word, J. M.; Prisant, M. G.; Richardson, J. S.; Richardson, D. C. *Proteins* **2003**, *50*, 437−450.
(54) Vriend, G. *J. Mol. Graph.* **1990**, *8*, 52−56, 29.
(55) Laskowski, R.; MacArthur, M.; Moss, D.; Thornton, J. *J. Appl. Crystallogr.* **1993**, *26*, 283−291.
(56) Esnouf, R. M. *J. Mol. Graph. Model.* **1997**, *15*, 132−134.
(57) Merritt, E. A.; Bacon, D. J. *Methods Enzymol.* **1997**, *277*, 505−524.